HHS Public Access

Author manuscript

Nat Cardiovasc Res. Author manuscript; available in PMC 2024 August 23.

Published in final edited form as:

Nat Cardiovasc Res. 2024 March ; 3(3): 343–355. doi:10.1038/s44161-024-00441-z.

Disruption of the *Uty* epigenetic regulator locus in hematopoietic cells phenocopies the profibrotic attributes of Y chromosome loss in heart failure

Keita Horitani[1,7,11], **Nicholas W. Chavkin**[1,2,11], **Yohei Arai**[1], **Ying Wang**[1,8], **Hayato Ogawa**[1,9], **Yoshimitsu Yura**[1,9], **Megan A. Evans**[1], **Jesse D. Cochran**[1,3], **Mark C. Thel**[1], **Ariel H. Polizio**[1], **Miho Sano**[1], **Emiri Miura-Yura**[1,10], **Yuka Arai**[1], **Heather Doviak**[1], **Arthur P. Arnold**[4], **Bradley D. Gelfand**[5], **Karen K. Hirschi**[2], **Soichi Sano**[1,6,11], **Kenneth Walsh**[1]

[1]Hematovascular Biology Center, Robert M. Berne Cardiovascular Research Center, University of Virginia School of Medicine, Charlottesville, VA, USA.

[2]Department of Cell Biology, University of Virginia School of Medicine, Charlottesville, VA, USA.

[3]Medical Scientist Training Program, University of Virginia School of Medicine, Charlottesville, VA, USA.

[4]Department of Integrative Biology and Physiology, University of California, Los Angeles, Los Angeles, CA, USA.

[5]Ophthalmology, Biomedical Engineering, Center for Advanced Vision Science (CAVS), University of Virginia School of Medicine, Charlottesville, VA, USA.

[6]Laboratory of Cardiovascular Mosaicism, National Cerebral and Cardiovascular Center, Osaka, Japan.

[7]Present address: Department of Medicine II, Kansai Medical University, Osaka, Japan.

[8]Present address: Department of Cardiology, Second Affiliated Hospital of Army Medical University, Chongqing, China.

[9]Present address: Department of Cardiology, Nagoya University Graduate School of Medicine, Nagoya, Japan.

Correspondence and requests for materials should be addressed to Soichi Sano or Kenneth Walsh. sano.soichi@ncvc.go.jp; kw9ar@virginia.edu.

Author contributions

S.S. and K.W. designed the experiments. K.H., N.W.C., Yohei A., Y.W., H.O., Y.Y., M.A.E., J.D.C., M.C.T., M.S., E.M.-Y., Yuka A., H.D., A.H.P. and S.S. performed the experiments. Y.W. performed statistical analyses. A.P.A., B.D.G. and K.K.H. provided scientific advice. S.S., N.W.C. and K.W. wrote the paper. All authors approved the final version of the paper.

Competing interests

The authors declare no competing interests.

Additional information

Extended data is available for this paper at https://doi.org/10.1038/s44161-024-00441-z.

Supplementary information The online version contains supplementary material available at https://doi.org/10.1038/s44161-024-00441-z.

Code availability Code used to analyze datasets was generated from available vignettes and tutorials. This code is available at https://github.com/nicholaschavkin/UTY_HF.

[10]Present address: Division of Diabetes, Department of Internal Medicine, Aichi Medical University School of Medicine, Nagakute, Japan.

[11]These authors contributed equally: Keita Horitani, Nicholas W. Chavkin, Soichi Sano.

Abstract

Heart failure affects millions of people worldwide, with men exhibiting a higher incidence than women. Our previous work has shown that mosaic loss of the Y chromosome (LOY) in leukocytes is causally associated with an increased risk for heart failure. Here, we show that LOY macrophages from the failing hearts of humans with dilated cardiomyopathy exhibit widespread changes in gene expression that correlate with cardiac fibroblast activation. Moreover, we identify the ubiquitously transcribed t et ratricopeptide Y-linked (*Uty*) gene in leukocytes as a causal locus for an accelerated progression of heart failure in male mice with LOY. We demonstrate that *Uty* disruption leads to epigenetic alterations in both monocytes and macrophages, increasing the propensity of differentiation into profibrotic macrophages. Treatment with a transforming growth factor-β-neutralizing antibody prevented the cardiac pathology associated with *Uty* deficiency in leukocytes. These findings shed light on the mechanisms that contribute to the higher incidence of heart failure in men.

The Y chromosome is gene sparse and can be lost from leukocytes in men in a phenomenon known as mosaic loss of the Y chromosome (LOY). This chromosomal loss increases as men age, with roughly 40% of men aged 70 years exhibiting LOY[1], thus representing the most prevalent known somatic mutation in humans. While the existence of LOY in the blood has been known for over half a century[2,3], its impact has largely been overlooked due to the relatively small number of Y chromosome genes expressed in nonreproductive tissues, leading to the presumption that their loss from blood cells would be clinically irrelevant. This notion is supported by the fact that the Y chromosome is mainly noncoding; it contains two pseudoautosomal regions (PARs) flanking the male-specific region of Y, which is split into a heterochromatic segment and a euchromatic segment, with only a small section surrounding the centromere coding for protein products from approximately 70 genes[4]. The potential roles of these genes beyond sex determination have not been well described.

In recent years, however, analyses of large biobanks with whole-genome sequencing datasets and detailed patient phenotypes have revealed associations between LOY and an increased risk of various age-related diseases in men, including various cancers, Alzheimer's disease and cardiovascular disease (CVD)[5–8]. Moreover, evidence has emerged suggesting that the Y chromosome contributes to the regulation of global gene expression and biological processes in leukocytes, in addition to determining biological sex[9]. Thus, LOY in leukocytes may be implicated in the development and progression of diseases through the alteration of immune cell function. Indeed, our recent research has substantiated a potential causal link between LOY in leukocytes and heart failure[8]. In both humans and mice, loss of the entire Y chromosome in leukocytes has been correlated with adverse cardiovascular outcomes. Notably, mice with hematopoietic LOY display exacerbated cardiac dysfunction with age and in response to pressure overload, largely due to enhanced profibrotic activity in cardiac macrophages that lack the Y chromosome. Despite the pervasive occurrence and substantial

clinical relevance of LOY, our understanding of the specific Y chromosomal genes and pathways that affect cardiac function remains incomplete.

A key question is whether the cardiovascular effects of LOY are simply a consequence of the aneuploid condition or whether the Y chromosome encodes genes that are required for cardiovascular homeostasis. In this study, we provide evidence for the latter hypothesis and identify *Uty* (ubiquitously transcribed tetratricopeptide repeat containing, Y-linked) as a critical Y chromosome gene, the deficiency of which might underpin LOY-related pathologies in the heart. *Uty* is an epigenetic regulator expressed in hematopoietic cells of both humans and mice. Notably, its deficiency in the monocyte–macrophage lineage in mice triggers an epigenetic rewiring toward a profibrotic phenotype. This shift results in enhanced cardiac fibrosis and exacerbated heart failure in mice, recapitulating our previous findings on the effects of hematopoietic LOY on heart failure in mice. The cardiac phenotype caused by *Uty* disruption can be prevented through the administration of transforming growth factor-β (TGFβ)-neutralizing antibodies, suggesting a potential druggable target and therapeutic strategy for LOY-related conditions.

Results

Cardiac macrophage LOY is associated with fibroblast activation

Our previous study in a mouse model of heart failure revealed that macrophages lacking the Y chromosome have a role in driving the progression of cardiac fibrosis and the reduction of cardiac output, in part through the differential expression of genes involved in macrophage polarization[8]. To investigate whether failing human hearts contain LOY macrophages that have unique transcriptional signatures compared to Y-containing macrophages and whether human cardiac LOY macrophages activate fibrotic pathways, we performed an analysis of three clinical single-cell RNA-sequencing (scRNA-Seq) datasets of cardiac biopsy samples from healthy patients and patients with dilated cardiomyopathy (DCM)[10–12]. High-quality cells with >2,000 reads from individual male patients were clustered and annotated by cell type, and leukocytes were further clustered and annotated by the expression of marker genes (Fig. 1a and Extended Data Fig. 1). LOY cells were defined as cells without expression of Y chromosome genes, which could be detected among all leukocyte clusters with a large percentage in macrophages (Fig. 1b and Extended Data Fig. 1). Analysis of differential gene expression revealed that 9.78% of detected transcripts (n = 25,958) were differentially expressed between Y-replete and LOY macrophages, most (~97%) of which were autosomal, documenting the widespread effect of LOY on macrophage gene expression (Fig. 1c,d). Next, fibroblast activation was investigated and correlated with the percentage of LOY in leukocytes in individual patients. The normalized expression of hallmark fibroblast activation genes (*POSTN*, *ACTA2*, *COL1A1*, *COL3A1*) was elevated in fibroblasts from patients with DCM compared to those from healthy patients (Fig. 1e). Comparing this measure of fibroblast activation with the percentage of LOY leukocytes in each healthy patient or patient with DCM revealed that a higher proportion of LOY significantly correlated with a higher degree of fibroblast activation (Fig. 1f) and a higher percentage of the myofibroblast subpopulation (Extended Data Fig. 1)[13,14]. Finally, Gene Ontology enrichment analysis of significantly variable genes between Y-replete and LOY

macrophages identified terms related to histone modification, leukocyte differentiation and activation, and pathways related to macrophage function (Fig. 1g). Together, these results suggest that the Y chromosome has a role in the regulation of activated macrophages in cardiac tissue, potentially affecting a broad range of autosomal genes through histone modification functions, to promote fibrosis in patients with DCM.

Deletion of Y genes promotes cardiac dysfunction in transverse aortic constriction

LOY in leukocytes has been associated with worse outcomes in heart failure, but it is not clear whether the observed phenotype is caused by the aneuploidy itself or the loss of specific Y chromosome genes in hematopoietic cells. To distinguish between these two hypotheses in heart failure, we used the XY*–XY*^{X} mouse model[15]. This model features a nonrecombinant Y chromosome variant (denoted 'Y*') that has sufficient Y chromosome genes and a recombinant Y chromosome variant (denoted 'Y*^{X}') that is largely deficient in Y chromosome genes, except for the PARs, which are necessary for pairing and recombination with the X chromosome during cell division. The system makes the deletion of nearly all Y chromosome genes possible without affecting the overall ploidy of cells (Fig. 2a). The Y*^{X} chromosome also contains a small subsegment of the non-PAR of the X chromosome (NPX), which is estimated to be <1% of the total NPX. Thus, this XY* (Y genes replete) and XY*^{X} (Y genes deficient) model enabled us to investigate whether the loss of Y genes is sufficient to recapitulate the effects of hematopoietic LOY on cardiac dysfunction in the absence of aneuploidy.

To validate this model, we performed real-time PCR analysis to examine the expression of Y chromosome-encoded genes in bone marrow cells isolated from XY* mice and XY*^{X} mice. Transcripts of Y chromosome genes, including *Eif2s3y* (eukaryotic translation initiation factor 2, subunit 3, structural gene Y-linked), *Ddx3y* (DEAD-box helicase 3 Y-linked), *Kdm5d* (lysine demethylase 5d) and *Uty*, were not detectable in bone marrow cells from XY*^{X} mice (Fig. 2b). Furthermore, no compensatory upregulation of X chromosome homologs was observed in these cells (Fig. 2c). To examine whether bone marrow cells from XY*^{X} mice have a fitness advantage over wild-type cells, we used a competitive bone marrow transplantation (BMT) strategy. Lethally irradiated mice were transplanted with bone marrow cells containing 50% CD45.2^{+} XY*^{X} cells (Y genes deficient) and 50% CD45.1^{+} XY cells (with normal Y chromosome). Mice transplanted with 50% XY* cells (Y genes sufficient) and 50% XY cells were used as controls. XY*^{X} cells did not undergo selective expansion over the time course of the experiments (Extended Data Fig. 2), consistent with our previous finding that hematopoietic cells lacking the entire Y chromosome do not show an obvious fitness advantage in mice[8].

Next, we investigated whether mice with hematopoietic cells lacking Y chromosome genes but maintaining euploidy (that is, XY*^{X}) had a worse outcome with heart failure. Experimental groups underwent transplantation with either XY*^{X} or XY* bone marrow cells. Mice were then subjected to pressure overload by performing transverse aortic constriction (TAC), in which a suture is placed around the ascending aorta to constrict the lumen and partially obstruct blood flow, resulting in increased pressure and workload on the heart (Fig. 2d). This model induces compensatory hypertrophy in the heart,

followed by long-term degenerative changes leading to decompensated heart failure[16,17]. Echocardiographic analysis revealed a greater decline in cardiac function in mice with hematopoietic XY*^{X} cells than in control mice (Fig. 2e). Moreover, there was elevated cardiac hypertrophy in mice with XY*^{X} blood cells after TAC, reflected by an increase in the ratio of heart weight to tibia length (Fig. 2f). These mice also displayed an increase in the ratio of lung weight to tibia length, indicative of lung congestion resulting from cardiac dysfunction (Fig. 2f). Transcriptional expression of markers of advanced heart failure (atrial natriuretic peptide A (*Nppa*) and the ratio of myosin heavy chains b/a (*Mhc b/a*)) were upregulated in the hearts of mice with hematopoietic XY*^{X} cells compared to that in the hearts of control hematopoietic XY* mice (Fig. 2g). Histological analysis revealed that mice with XY*^{X} cells displayed increased fibrosis in the left ventricle of the heart after TAC, as evidenced by greater interstitial and perivascular fibrosis (Fig. 2h). Collectively, these findings show that the deficiency of the Y chromosome gene-encoding region is sufficient to contribute to the cardiac phenotype observed in LOY mice after TAC.

Y gene screen implicates *Uty* in LOY-mediated cardiac effects

Although most genes encoded by the male-specific region of Y in the C57BL/6J strain of *Mus musculus* are predominantly expressed in the tissues of the reproductive system, four genes are expressed ubiquitously across tissue types (*Ddx3y*, *Eif2s3y*, *Kdm5d* and *Uty*)[18]. These four genes are expressed in recruited cardiac macrophages, and their expression is undetectable in the clustered regularly interspaced short palindromic repeat (CRISPR)-based LOY mouse model described previously[8]. In the XY*–XY*^{X} system, *Ddx3y*, *Eif2s3y*, *Kdm5d* and *Uty* expression could be detected in the cardiac macrophages of control mice but not in the macrophages of XY*^{X} mice (Fig. 2b), consistent with a previous study[19]. Furthermore, while *EIF2S3Y* is not located on the human Y chromosome, the expression of the *DDX3Y*, *KDM5D* and *UTY* genes could be detected in human cardiac macrophages within healthy hearts from the generated scRNA-Seq database (Extended Data Fig. 3).

To assess whether the loss of any of these four mouse Y-linked, non-PAR genes could contribute to impaired cardiac function in mice, hence recapitulating hematopoietic LOY, we used the CRISPR/CRISPR-associated 9 (Cas9) method to create donor hematopoietic stem cells with targeted disruption of these individual genes and, thereby, to generate mice with hematopoietic system-specific gene knockout through BMT[20]. In this approach, donor bone marrow cells from ROSA-Cas9 knockin mice[21], which constitutively express the Cas9 endonuclease, were used to uncouple the *Cas9* gene from the lentivirus vector for encoding the guide RNAs (gRNAs) and to maximize the effectiveness of gene editing. Cas9^{+} bone marrow cells were transduced with lentiviral vectors encoding the individual gRNAs ex vivo for 16–20 h and then transplanted into wild-type mice that had been conditioned by irradiation (Fig. 3a). Transduction was determined by assessing the lentivirus-encoded red fluorescent protein (RFP) reporter gene expression in various blood fractions by flow cytometric analysis (Extended Data Fig. 4a). Mice with hematopoietic cell disruption of the *Eif2s3y*, *Ddx3y*, *Kdm5d* or *Uty* gene were assessed for the efficiency of gene editing using Tracking of Indels by Decomposition (TIDE) analysis. The TIDE results showed that a portion of the CRISPR-targeted locations had insertion or deletion mutations, with most of these mutations giving rise to frameshift mutations (Extended Data Fig. 4b–e).

The transplantation of these cells led to approximately 60% engraftment of gene-edited or control cells (Extended Data Fig. 4f). The disruption of any of these genes did not lead to observable changes in general hematopoietic parameters, including no significant differences in the total number of white blood cells, hemoglobin concentration or platelet counts between gene-edited mice and control mice (Extended Data Fig. 5).

The cardiac response of these mice to pressure overload-induced cardiac injury was then assessed to determine whether the disruption of individual genes could recapitulate the reduction in cardiac function observed in the LOY models[8]. Editing of the *Ddx3y*, *Kdm5d* or *Eif2s3y* locus in hematopoietic cells did not produce detectable consequences on cardiac function at baseline or in response to TAC surgery, and there were no effects on relative heart weight or lung weight (Extended Data Fig. 6). In contrast, editing of the *Uty* locus in hematopoietic cells within exon 1 led to an increase in heart weight and lung congestion in response to TAC (Fig. 3b). Before the mice were killed, serial echocardiographic analysis also revealed that *Uty* disruption led to a marked reduction in cardiac function in response to TAC (Fig. 3c). Based on these findings, it appears that the disruption of the *Uty* locus in hematopoietic cells can lead to cardiac dysfunction in response to TAC in a manner similar to that observed in the XY*–XY*^{X} system (Fig. 2) or by ablation of the entire Y chromosome through CRISPR/Cas9 editing[8], suggesting that the *Uty* gene is a candidate locus responsible for the cardiac phenotype of LOY mice.

Disrupting *Uty* in leukocytes accelerates cardiac dysfunction

Uty gene trap (*Uty*^{GT}) mice were used to test further whether *Uty* gene disruption in hematopoietic cells worsens cardiac dysfunction after TAC (Fig. 3d). While the CRISPR/Cas9 disruption of *Uty* targeted exon 1, *Uty*^{GT} mice were engineered by placing an inactivating gene trap in the fourth intron of the *Uty* gene[22]. The absence of *Uty* transcripts in *Uty*^{GT} mice was verified in whole bone marrow cells, whole peripheral blood cells and peritoneal macrophages (Fig. 3e and Extended Data Fig. 7a). The expression of *Utx* (homolog of *Uty* on the X chromosome), *Ddx3x*, *Eif2s3x* and *Kdm5c* was unaffected by the disruption of *Uty* in these mice (Extended Data Fig. 7b).

Mice underwent BMT with either *Uty*^{GT} or control cells and were then assessed for the severity of cardiac dysfunction after TAC. In these experiments, the thoraxes of recipient mice were shielded during the irradiation preconditioning to minimize the confounding effects of radiation on the heart[23]. By using this strategy, blood donor chimerism levels ranging from 50% to 70% were achieved[24]. As observed in the CRISPR/Cas9-based screen that targeted the *Uty* locus (Fig. 3a–c), mice transplanted with *Uty*^{GT} hematopoietic cells displayed greater reductions in cardiac function, as determined by echocardiographic analysis after TAC, and elevated cardiac hypertrophy, as indicated by an increase in the ratio of heart weight to tibia length (Fig. 3f,g). *Uty* deficiency did not affect the circulating populations of leukocytes, nor did it affect body weight or lung weight in the TAC model (Extended Data Fig. 7c–e).

Mice transplanted with *Uty*^{GT} hematopoietic stem cells exhibited trends of increased expression of transcripts encoding *Nppa* and a higher *Mhc b/a* ratio in their hearts compared to control mice (Fig. 4a). The myocardial transcript levels of fibrosis marker genes,

including collagen 1a1 (*Col1a1*), collagen 3a1 (*Col3a1*) and matrix metalloproteinase 2 (*Mmp2*), were elevated in mice transplanted with Uty^{GT} cells, suggesting that hematopoietic *Uty* disruption leads to increased myocardial fibrosis (Fig. 4b). Furthermore, flow cytometric analysis of heart cells revealed that the number of $CD45^{-}CD31^{-}mEF^{-}SK4^{+}$ fibroblasts was higher in the hearts of TAC-treated mice transplanted with hematopoietic Uty^{GT} cells compared to control mice (Fig. 4c). Consistent with these findings, histological analysis revealed greater fibrosis in the left ventricle of mice transplanted with Uty^{GT} bone marrow cells after TAC (Fig. 4d); in contrast, there was no detectable difference in the number of cardiac endothelial cells (defined as $CD45^{-}CD31^{+}$) (Fig. 4e). Taken together, these results provide additional support for the hypothesis that hematopoietic disruption of the *Uty* locus accelerates cardiac dysfunction in an experimental model of myocardial fibrosis.

To extend these analyses, a series of experiments used *Ddx3y*-deficient mice in the BMT/TAC model (Extended Data Fig. 8a)[25]. These mice lack *Ddx3y* transcript expression in the bone marrow, but the expression of *Ddx3x* and other X chromosome-encoded genes was unaffected (Extended Data Fig. 8b,d). In contrast to findings with the Uty^{GT} bone marrow, transplantation with the *Ddx3y*-deficient knockout bone marrow had no effect on cardiac function, heart weight or other markers of cardiac failure in the TAC model (Extended Data Fig. 8d–f).

Uty regulates the fate of cardiac monocytes and macrophages

Given the role of *Uty* as an epigenetic regulator[26,27], we investigated the epigenetic features of Uty^{GT}-deficient immune cells in the heart under conditions of pressure overload. In the BMT/TAC model, multimodal single-cell analysis was conducted on the Uty^{GT} immune cells within the heart, wherein we assessed the transcriptome and chromatin accessibility at a single-cell resolution (Fig. 5a). In these assays, Uty^{GT} mice were used as bone marrow cell donors and recipient mice underwent chest shielding during irradiation to protect the endogenous immune cell niches within the myocardium. To examine immune cells that were recruited to the hearts after TAC and discriminate the progeny of transplanted cells from those of recipient cells, we used the CD45 congenic mouse system, in which CD45.2 is used as a marker of donor leukocytes (Uty^{GT} or wild-type) and CD45.1 as a marker of recipient leukocytes (wild-type). In these experiments, $CD45.2^{+}$ immune cells were isolated from the hearts of chimeric mice at 7 days after TAC. These cells then underwent single-cell multiomics analysis of isolated nuclei, which included combined scRNA-Seq analysis and single-cell assay for transposase-accessible chromatin sequencing (scATAC-Seq) analysis of nucleic acid material isolated from individual nuclei, to investigate their gene expression and chromatin accessibility profiles (Fig. 5a). Quality control metrics showed high ATAC depth, peak counts and enrichment of chromatin accessibility at transcriptional start sites (TSSs), and visualization of the coverage of the *Uty* locus confirmed reduction in chromatin activity around the Uty^{GT}-edited locus (Extended Data Fig. 9a,b).

Dimensionality reduction on scATAC peaks allowed for the clustering of control versus Uty^{GT} donor immune cell populations that were annotated based on gene expression from scRNA-Seq (Fig. 5b and Extended Data Fig. 9c,d). Based on the differential

chromatin availability around genes, the macrophage populations exhibited distinct clusters in UMAP plots according to the expression of profibrotic and proinflammatory marker genes (Extended Data Fig. 9e). Multimodal single-cell analysis revealed a higher number of cardiac macrophages in hematopoietic *Uty*-deficient mice than in control mice (Extended Data Fig. 10a). This observation was corroborated by flow cytometric analysis of macrophage content (Extended Data Fig. 10b). Consistent with this observation, analysis of differential gene expression revealed an increase in myeloid chemotaxis receptors and related Gene Ontology pathways in the pooled Uty^{GT} monocytes and macrophages (Extended Data Fig. 9c,d). This differential gene expression analysis revealed similar enrichment of the same Gene Ontology terms identified in the human LOY macrophages from patients with DCM (Extended Data Fig. 10e versus Fig. 1g), further implicating the potential importance of the macrophage population in mediating the effects of *Uty* loss. However, the shallow scRNA read coverage, likely due to the optimization of scATAC coverage and related limitations in the multiome analysis, precluded further examination of gene expression.

The investigation of chromatin availability near TSSs can provide insights into cellular identity and function. Thus, the specific epigenetic features associated with *Uty* disruption were assessed. Using previously identified transcriptomic signatures of fibrotic and inflammatory cardiac macrophages from our previously published mosaic LOY scRNA-Seq analysis of TAC-related hearts[8], we observed that Uty^{GT} macrophages exhibited greater enrichment in the fibrotic signature compared to their control counterparts, whereas no significant differences were observed in inflammatory signatures (Fig. 5c). In addition to macrophages, monocytes recruited to the heart in response to pressure overload injury also displayed a significant enrichment in chromatin availability at TSSs of fibrotic genes. This finding suggests that the epigenetic rewiring caused by *Uty* disruption, which gives rise to a fibrotic gene signature, occurs in the early monocytic stage and precedes macrophage differentiation when robust LOY-mediated changes in gene transcription are observed[8].

Consistent with *Uty*'s function as an epigenetic regulator, an analysis of the differential chromatin accessibility around genes in *Uty*-deficient monocytes and macrophages revealed a distinctly different gene profile compared to control cells (Fig. 5d). In this context, increased chromatin accessibility proximal to genes typically suggests that these genes are actively being transcribed. A Gene Ontology enrichment analysis revealed that *Uty*-deficient monocytes and macrophages display differential gene accessibility profiles related to several biological processes that are critical for the development of cardiac fibrosis, including greater accessibility around genes associated with the 'platelet-derived growth factor signaling pathway', 'regulation of tissue remodeling', 'extracellular matrix organization' and 'regulation of cellular response to TGFβ stimulus' (Fig. 5e), consistent with the hypothesis that *Uty* deficiency promotes macrophage polarization toward a fibrotic phenotype. Further supporting a propensity toward fibrotic polarization and away from an inflammatory phenotype, genes with reduced accessibility in *Uty*-deficient monocytes and macrophages were associated with inflammatory pathways, including 'chemokine production', 'tumor necrosis factor-mediated signaling pathway' and 'cytokine production involved in immune response' (Fig. 5e). Additionally, analysis of transcription factor-binding sequences in the chromatin accessibility peaks revealed distinct motifs that were preferentially found in

chromatin-accessible regions in Uty^{GT} monocytes and macrophages (Fig. 5f). These motifs were related to profibrotic transcription factors, such as Elk3, Cux1 and Ctcf, and were also identified by the previous transcriptomic analysis of LOY[8], providing further evidence that the *Uty* locus has a role in accelerating cardiac fibrosis in a manner consistent with the LOY condition (Fig. 5g). In contrast, there was diminished enrichment of transcription factor motifs associated with a proinflammatory gene regulatory network in the *Uty*-disrupted versus control monocytes and macrophages, including the binding motifs for the family of Jun and Fos transcription factors (Fig. 5g). Collectively, these findings indicate that the *Uty* locus on the Y chromosome has a critical role in modulating the balance between fibrotic and inflammatory responses of monocytes and macrophages in the myocardium.

TGFβ is necessary for Uty^{GT}-mediated cardiac dysfunction

To investigate the functional impact of the profibrotic epigenetic rewiring in Uty^{GT} myeloid cells, we performed TAC in mice transplanted with either Uty^{GT} or wild-type cells and treated them with either an immunoglobulin G (IgG) control or a monoclonal antibody that targets TGFβ (Fig. 6a). Through sequential echocardiographic analysis, it was observed that treatment with the anti-TGFβ monoclonal antibody largely reversed the accelerated cardiac dysfunction observed in mice with hematopoietic Uty^{GT} cells (Fig. 6b). Additionally, the anti-TGFβ antibody prevented the increase in serum brain natriuretic peptide (BNP) concentration, heart weight and lung congestion that were elevated in hematopoietic Uty^{GT} mice exposed to TAC (Fig. 6c,d). TGFβ neutralization also suppressed the increase in fibroblast number and extracellular matrix deposition in the heart that was associated with the Uty^{GT} condition, but it did not alter the number of endothelial cells (Fig. 6e).

Discussion

It has been historically thought that the Y chromosome exerts minimal effects on nonreproductive tissues due to its limited gene content and the view that Y-linked genes are predominantly involved in the development of the male reproductive system. The prevailing assumption has been that nonreproductive tissues are primarily regulated by sex differences through the indirect impact of sex hormones rather than the direct participation of Y chromosome-encoded genes. However, emerging research has highlighted the importance of the Y chromosome in extragonadal tissues[28], prompting a reevaluation of this notion. Notably, the phenomenon of LOY in leukocytes has been associated with a diminished lifespan and an increased risk of various age-related diseases, underscoring the potential physiological roles of the Y chromosome beyond sex determination and spermatogenesis[29].

Recently, our research uncovered that men with hematopoietic LOY are more likely to experience greater mortality from heart failure[8]. Our study also revealed that hematopoietic LOY has a causal role in cardiac dysfunction evident under conditions of acute pressure overload and physiological aging in mice[8]. Mechanistic studies showed that macrophages lacking the Y chromosome exhibit a greater propensity to adopt a profibrotic phenotype characterized by increased expression of cytokines such as TGFβ1 and an upregulation of the TGFβ1 receptor (TGFBR) signaling pathway. Consistent with this, it was found that LOY in the blood is associated with various cardiovascular conditions in which TGFBR

signaling can have a prominent role[8]. Also consistent with these findings, it was recently reported that LOY monocytes display elevated TGFBR signaling in men with impaired long-term survival after transcatheter aortic valve replacement[7]. In the current study, we show that LOY macrophages are associated with increased fibroblast activation in the myocardium of men with DCM. Single-cell analysis of these macrophages revealed widespread changes in the transcription of autosomal genes, with an enrichment of genes associated with elevated TGFBR signaling and fibroblast activation. Thus, the identification of Y chromosome loci that confer these far-reaching genomic actions can provide an important step forward in addressing the mechanisms by which hematopoietic LOY contributes to CVD.

To define the mechanisms by which LOY confers a pathological phenotype to the myocardium, we first evaluated a second LOY model that uses an altered chromosome largely lacking the Y chromosome gene-coding regions (except for the PARs). As mosaic LOY involves the loss of an entire chromosome, it was unclear whether mosaic LOY-related phenotypes are caused by aneuploidy per se or by the loss of functional Y chromosome-encoded genes. Aneuploidy itself can alter cell function by directly affecting gene expression or by triggering other physiological responses[30]. Alternatively, the lack of Y chromosome genes with histone modification functions could explain the large transcriptional changes observed in cardiac macrophages with LOY. Therefore, we used XY*^{X} mice in experiments because this model permits evaluating the gene-encoding regions of the Y chromosome while maintaining ploidy. Following the BMT of XY*^{X} cells, these mice exhibited a similar cardiac dysfunction phenotype in the TAC model as was observed through the ablation of the entire Y chromosome in hematopoietic cells by CRISPR gene editing. Thus, these experiments provide evidence that the loss of gene-encoding regions on the Y chromosome underpins the myocardial LOY phenotype.

Based on the findings from the XY*–XY*^{X} system, we carried out a screening of potential Y chromosome genes that might contribute to the acceleration of heart failure in mice with LOY. We identified four coding genes (*Kdm5d*, *Ddx3y*, *Uty*, *Eif2s3y*) that are expressed in cardiac macrophages. Among these, *Kdm5d* and *Uty* are notable due to their roles as epigenetic regulators that could account for the widespread changes observed in autosomal gene expression caused by LOY[9]. Although the individual disruption of *Kdm5d*, *Ddx3y* or *Eif2s3y* by CRISPR gene editing had no detectable effect on cardiac dysfunction in the TAC model, the disruption of *Uty* exacerbated the cardiac dysfunction and hypertrophy observed in the TAC model. The importance of the *Uty* locus in the LOY effect was corroborated by experiments showing that mice transplanted with *Uty*^{GT} bone marrow cells exhibited exacerbated cardiac dysfunction in response to TAC compared to their wild-type counterparts. *Uty* is a member of the histone demethylase protein family of epigenetic regulators. While its demethylase activity is lower than that of its paralog, *Utx*, recent studies show that *Uty* can also modulate epigenetic processes through phase separation-mediated regulation of gene expression[26].

Consistent with the LOY phenotype, single-cell multiomics analysis revealed that hematopoietic *Uty* disruption promotes accessibility to genes related to ‘macrophage migration’, ‘tissue remodeling’, ‘extracellular matrix organization’, ‘TGFβ signaling’, etc., within cardiac macrophages. Conversely, *Uty* disruption diminished the chromatin

accessibility of genes related to inflammation. These data align with our findings that hematopoietic *Uty*^{GT} mice, as well as the XY*^{X} and CRISPR/Cas9 models of LOY, display increased cardiac fibrosis following TAC. Intriguingly, the changes in chromatin accessibility triggered by *Uty* disruption are not restricted to differentiated cardiac macrophages. Similar alterations were also observed in *Uty*^{GT} monocytes that do not exhibit robust changes in gene expression at this stage[8]. These findings provide evidence that the process of epigenetic rewiring commences in hematopoietic cells before the stage of cardiac macrophage differentiation (Supplementary Fig. 1). This observation prompts additional questions: could similar epigenetic changes take place at even earlier stages, such as within progenitor cells or hematopoietic stem cells? If so, does *Uty* deficiency (and, by extension, LOY in leukocytes) accelerate the progression of multiple fibrotic diseases through a common epigenetic regulatory mechanism that may be initiated in the bone marrow? These questions warrant further investigations.

Our findings causally link a Y chromosome-encoded gene (*Uty*) to nonischemic heart failure. While we present multiple lines of evidence supporting a role for *Uty* in cardiac dysfunction and fibrosis, the results of our study do not diminish the potential impact of other Y chromosome regions that might also contribute to CVD or other LOY-associated diseases in older men. This notion is supported by two recent studies showing that LOY can promote cancer progression. For instance, LOY or deficiency of the histone 3 lysine 4 demethylase Kdm5d has been shown to promote the clonal expansion of hematopoietic stem cells and leukemogenesis in mice[31]. Abdel-Hafiz et al.[32] recently reported that Y chromosome-deficient tumors have more aggressive growth in a bladder cancer model, and these effects could also be observed when knocking out either *UTY* or *KDM5D*. This study also showed that LOY in cancer cells can promote tumor growth through immune suppression of the tumor microenvironment. These data are generally consistent with our finding that LOY reduces inflammatory responses, both in the current study and our previous work[8]. Collectively, these findings suggest that, in addition to fibrotic heart disease, LOY may affect disparate diseases through similar regulatory mechanisms that can be modulated by the small group of ubiquitously expressed Y chromosome-encoded genes. Therefore, a more comprehensive grasp of the Y chromosome's roles in the pathogenesis of various diseases will likely provide a better understanding of morbidity and mortality in men.

Methods

Study approval

The protocols for animal experiments described in this article were approved by the Institutional Animal Care and Use Committee of the University of Virginia.

Analysis of publicly available human cardiac scRNA-Seq datasets

Previously generated and published processed scRNA-Seq matrices of gene expression in individual cells, obtained through cell or nuclei isolation from human cardiac tissue, were acquired through publicly available repositories (National Center for Biotechnology Information Gene Expression Omnibus (NCBI GEO) accession nos. GSE183852 and

GSE145154, Broad Institute Single Cell Portal accession no. SCP1303)[10–12]. Seurat v4 was used to process and analyze these datasets[33]. Cells from individual studies were integrated using the reciprocal principal component analysis integration pipeline to generate a single dataset comprising 33,194 cardiac leukocytes from male patients. Clustering and UMAP (Uniform Manifold Approximation and Projection) dimensionality reduction were performed and plotted, and the relative expression of genes (*PTPRC*, *CD68*, *CD14*, *UTY*, *DDX3Y*, *KDM5D*) was plotted over the UMAP positions. Analysis of differential gene expression between Y-replete and LOY cardiac macrophages was performed (using the FindMarkers function in Seurat) on all genes expressed in >0.1% of cells, and Gene Ontology analysis was performed on genes with $P > 0.05$ and differential expression >5%.

Mouse strains

B6 mouse strain (C57BL/6J) and Rosa26Cas9 knockin mouse strain (B6(C)-*Gt(ROSA)26Sor*$^{em1.1(CAG-cas9*,-EGFP)Rsky}$/J) were purchased from the Jackson Laboratory (stock nos. 000664 and 028555, respectively). *Uty*-knockout mouse strain (B6.129P2(CD1)-*Uty*$^{Gt(XS0378)Wtsi}$/Mmnc) was purchased from the Mutant Mouse Resource and Research Centers (stock no. 037420-UNC). The *Ddx3y*-deficient mice B6D2-*Ddx3y*^{em2Osb} were described previously[25]. XY* mice were described previously[15] and bred at the University of Virginia. Progeny of XX and XY* mice that were either XY* (control) or XY*^{X} (loss of Y genes) were used to obtain donor hematopoietic stem cells for BMT experiments. Male mouse strains were kept in a specific pathogen-free animal facility on a 12-h light/12-h dark schedule, with unlimited access to food and water, an ambient temperature of 21.5 °C (acceptable range 20–26 °C) and an ambient humidity of 40% (acceptable range 30–70%).

Plasmids

Single gRNAs (sgRNAs) targeting the Y chromosome genes (*Eif2s3y*, *Ddx3y*, *Kdm5d*, *Uty*) were designed with in silico tools (https://portals.broadinstitute.org/gpp/public/analysis-tools/sgrna-design ; https://www.benchling.com), and the control gRNA was nontargeting. Supplementary Table 1 contains a list of sgRNA sequences. Single-stranded sgRNA sequences were annealed and cloned into the pLKO.sgRNA. EFS.tRFP vector following restriction digestion with Esp3I. Sanger sequencing with U6 primer was used to confirm successful cloning. Plasmids were purchased from Addgene (pLKO5.0.sgRNA.EFS.tRFP, plasmid 57823; psPAX2, plasmid 12260; and pMD2.G, plasmid 12259). To characterize indel mutations, we performed pooled DNA sequencing, followed by TIDE analysis using sorted cells from mouse peripheral blood (http://tide.nki.nl) (Supplementary Table 1).

Bone marrow reconstitution with ex vivo genome-edited lineage-negative cells

sgRNAs were delivered lentivirally to bone marrow lineage-negative cells obtained from ROSA26Cas9 knockin mice, as previously described[34].

Lentivirus production.

Collagen solution (0.005%) was applied to coat six-well culture plates at 37 °C and 5% CO_2 for 30 min. Human embryonic kidney (HEK) 293T cells (1×10^6) were seeded into each well and incubated for 2 h at 37 °C and 5% CO_2. The plasmids (0.9 mg of

pLKO5.0.sgRNAs.EFS.tRFP, 0.6 mg of psPAX2 and 0.3 mg of pMD2.G per well) were cotransfected to HEK 293T cells using PEI MAX (Polysciences, cat. no. 24765–1), and the cell culture medium was changed 3 h after transfection. Forty-eight hours after changing the medium, the culture supernatant was collected and centrifuged at 3,000*g* for 15 min to remove free-floating cells. Following filtration through a 0.45-μm filter, virus particles were concentrated by ultracentrifugation for 3 h at a speed of 72,100*g* at rmax. The viral pellet was suspended in StemSpan medium (STEMCELL Technologies, cat. no. 09600) without aeration and maintained at −80 °C. A Lenti-X quantitative reverse transcription followed by PCR (qRT–PCR) titration kit (Clontech, cat. no. 631235) was used to measure the titer of lentiviral particles.

Isolation of lineage-negative cells and lentivirus transduction.

Lineage-negative cells were purified from the bone marrow of Rosa26Cas9 knockin mice using a lineage cell depletion kit (Miltenyi Biotec, cat. no. 130–090-858). These cells were incubated in StemSpan medium for 1.5 h at 37 °C, followed by lentivirus transduction in the presence of 20 ng ml^{-1} thrombopoietin, 50 ng ml^{-1} stem cell factor 1 and 4 mg ml^{-1} polybrene for 16 h at 37 °C. Cells were washed and resuspended in RPMI medium and transplanted into lethally irradiated wild-type mice through the retro-orbital vein, as described below.

BMT.

Total body irradiation is commonly used before hematopoietic stem cell transplantation to achieve high levels of hematopoietic stem/progenitor cells for engraftment, as we did in the screening of Y chromosome genes in the above section. However, this preconditioning has various undesired consequences outside the hematopoietic system. Irradiation has been shown to cause inflammation, damage and fibrosis to a number of organ systems, including the skin, kidneys, lungs, brain and heart. In addition, exposure of the thorax to irradiation considerably replaces the resident cardiac macrophages with circulating monocyte-derived macrophages. This could substantially modify the disease sequelae under study. To eliminate these confounding effects, we used shielded irradiation to protect the hearts from radiation exposure. We used lead plates to cover the chest of mice during irradiation, as described previously[35]. Briefly, 8-week-old mice with chest shields were lethally irradiated using two exposures to 5.5-Gy irradiation 4 h apart, followed by reconstitution of hematopoietic stem cells by retro-orbital injection of 5 million cells per mouse.

TAC

The TAC procedure was carried out as previously described[8]. Briefly, isoflurane-anesthetized mice aged 12–16 weeks were subjected to a 27-gauge blunt-needle ligation of the transverse thoracic aorta between the innominate artery and the left common carotid artery; control mice underwent the same operation but without constriction. Investigators were blinded to the mouse genotype before performing the surgery on each group of mice.

TGFβ inhibition

Intraperitoneal injections of an anti-TGFβ antibody or IgG control (Bio X Cell, cat. nos. BP0057 and BP0083, respectively) were used to suppress TGFβ signaling. Each animal received 5 mg kg^{-1} of antibody every 3 days, starting 3 days before the TAC procedure and continuing for 4 weeks.

Echocardiography

The Vevo 2100 ultrasound system equipped with an MS550D probe (VisualSonics, Fujifilm) was used to assess cardiac function before and after TAC surgery at designated time points. Mice were placed supine on a heated platform, and their chest fur was removed using a depilatory cream after they were anesthetized with isoflurane inhalation (5% during induction, 1% during maintenance). With the heart rate maintained at 500–600 bpm, posterior wall thickness (mm), left ventricular systolic volume (μl), left ventricular end-diastolic volume (μl) and fractional shortening (%) were measured from M-mode tracing images obtained by a short-axis view. An investigator who was blinded to the mouse identity conducted the measurements and analyses using Vevo LAB software (VisualSonics, Fujifilm).

Flow cytometric analysis

To conduct flow cytometric analysis, we used the specific antibodies listed in Supplementary Table 2. Data acquisition was performed with the BD LSRFortessa flow cytometer (BD Biosciences) through the University of Virginia Flow Cytometry Core (Research Resource Identifier (RRID): SCR_017829), and the resulting data were analyzed using FlowJo software (BD Biosciences).

Peripheral blood samples were collected from the retro-orbital vein into K2EDTA-added BD Microtainer blood collection tubes (BD Biosciences, cat. no. 365974). Red blood cells (RBCs) were lysed with eBioscience 1× RBC lysis buffer (Thermo Fisher Scientific, cat. no. 00–4333-57) for 5 min on ice, followed by incubation with fluorochrome-conjugated antibodies for 20 min at room temperature in the dark. Neutrophils, monocytes, B cells, $CD4^+$ T cells, $CD8^+$ T cells and RFP^+ cells were identified using specific markers: $CD115^-Ly6G^+$ (neutrophils), $CD115^+Ly6G^-Ly6C^{hi}$ ($Ly6C^{hi}$ monocytes), $CD115^+Ly6G^-Ly6C^{low}$ ($Ly6C^{low}$ monocytes), $CD115^-Ly6G^-B220^+$ (B cells), $CD115^-Ly6G^-CD3e^+CD4^+$ ($CD4^+$ T cells) and $CD115^-Ly6G^-CD3e^+CD8^+$ ($CD8^+$ T cells). When using congenial strains, donor leukocytes were distinguished from recipient leukocytes by the markers CD45.2 and CD45.1.

Hearts were flushed with cold PBS from the apex and then excised. After the removal of the right ventricles, the left ventricles were minced and digested. Heart tissue was subsequently homogenized, and a single-cell suspension was obtained. After dead cell staining, cells were incubated with fluorochrome-conjugated antibodies and cell numbers were determined using 123count eBeads Counting Beads (Invitrogen, cat. no. 01–1234-42). Neutrophils, monocytes, macrophages, endothelial cells, fibroblasts and RFP^+ cells were identified using specific markers: $CD45^+CD64^-Ly6G^+$ (neutrophils), $CD45^+CD64^+Ly6G^-Ly6C^{hi}$ ($Ly6C^{hi}$ monocytes),

$CD45^+CD64^+Ly6G^-Ly6C^{low}$ (macrophages), $CD45^-CD31^+mEF^-SK4^-$ (endothelial cells) and $CD45^-CD31^-mEF^-SK4^+$ (fibroblasts).

Histological measurements

Heart tissues were collected at the indicated time points after TAC. Hearts were perfused with cold PBS from the apex and fixed in 10% formalin at 4 °C overnight. Samples were embedded in paraffin, and 7-μm-thick sections were processed. Following deparaffinization and rehydration, sections were stained with picrosirius red using freshly made staining solution, which included 1.2% by weight picric acid in water, 0.1% by weight Fast Green FCF and 0.1% by weight Direct Red 80 dissolved in PBS (Sigma-Aldrich, cat. nos. 197378, F7252 and 365548, respectively) for 1 h at room temperature. Sections were dehydrated after a quick wash in distilled water. The slides were mounted using a permanent mounting medium and coverslips. To quantify fibrosis, we examined images using the ImageJ program (National Institutes of Health). The amount of myocardial fibrosis was quantified as a proportion of the total left ventricular area.

Biochemical analysis

Mouse serum was extracted from clotted blood. In brief, peripheral blood was drawn from the retro-orbital vein and collected in clot activator- and serum separation gel-added BD SST Microtainer tubes (BD Biosciences, cat. no. 365967). The tubes were inverted five times and then centrifuged for 10 min at 6,000*g*, leaving the serum above the gel. The serum was snap frozen and stored at −80 °C until use. The BNP enzyme immunoassay kit (RayBiotech, cat. no. EIAM-BNP-1) was used to measure serum BNP levels.

Single-cell multiomics of recruited cardiac leukocytes

Cell isolation and sequencing.—Cardiac immune cells derived from BMT were isolated by tissue digestion and single-cell dissociation of cardiac tissue at 7 days after TAC, as previously described[8]. Briefly, hearts from control or Uty^{GT} BMT mice were isolated 7 days after TAC from three mice in each condition; cardiac tissue was digested using a digestion solution containing collagenase I (450 U ml^{-1}), collagenase XI (125 U ml^{-1}), hyaluronidase (450 U ml^{-1}) and DNAse I (60 U ml^{-1}) with subsequent homogenization; and live BMT-derived cardiac immune cells were isolated by fluorescence-activated cell sorting for the DAPI-$CD45.2^+$ population. Single-cell suspensions were then pooled between three mice at equal proportions. Nuclei were isolated from single-cell suspensions by washing once in cell buffer (PBS with 0.4% BSA), pelleting and resuspending in lysis buffer (10 mM Tris–HCl (pH 7.4), Sigma, cat. no. T2194l; 10 mM NaCl, Sigma, cat. no. 59222C; $MgCl_2$, Sigma, cat. no. M1028; 0.1% Tween-20; 0.1% Nonidet P40 substitute, Sigma, cat. no. 74385; 0.01% digitonin, Thermo Fisher Scientific, cat. no. BN2006; 1% MACS BSA, Miltenyi Biotec, cat. no. 130–091-376; in nuclease-free water) for 3 min on ice. Next, nuclei were washed once in wash buffer (same as lysis buffer but without Nonidet P40 substitute or digitonin) and resuspended in nuclei buffer (10x Genomics, cat. no. PN-2000153). Samples of nuclei were processed for single-cell multiomics library preparation using the Chromium Next GEM Single Cell Multiome ATAC + Gene Expression kit from 10x Genomics. Subsequent sequencing of ATAC and gene expression libraries was performed separately

using the NextSeq 2000 sequencer and P3 sequencing reagents from Illumina, according to validated standard operating procedures established and performed by the University of Virginia Genome Analysis and Technology Core (RRID: SCR_018883). As the analyzed cells were all mononuclear, results from single nuclei were assumed to correspond to the analysis of single cells.

Bioinformatics analysis.—Sequencing outputs from scATAC and gene expression datasets from BMT-derived control and *Uty*^{GT} immune cells were computationally aligned and integrated for downstream analysis. Sequencing reads were aligned to the mm10 mouse reference genome by Cell Ranger ARC: FASTQ files were generated using 'cellranger-arc mkfastq'; sequencing results were aligned to the mm10 reference genome using 'cellranger-arc count'; and datasets from control and *Uty*^{GT} immune cells were combined using 'cellranger-arc aggr'. A total of 17,325 cells were analyzed. The combined single-cell multiomics dataset was analyzed using Seurat v4.0.6 (ref. 33) and Signac v1.9 (ref. 36) software and pipelines. Filtering of cell quality parameters was performed to keep cells with ATAC counts between 500 and 60,000, RNA counts between 50 and 1,500, nucleosome signal <2 and transcriptional start site enrichment >1. After filtering, 16,341 cells were available for analysis. Peaks were called from ATAC reads using MACS2 (ref. 37) through Signac software. Seurat and Signac pipelines were used to perform gene normalization and scaling through SCTransform, UMAP dimensionality reduction, cell clustering and linking of peaks to genes. Gene expression was imputed using MAGIC[38]. Transfer and integration of previous scRNA-Seq datasets of mouse leukocytes after TAC[8] were performed using Seurat and Signac pipelines to score cells based on validated transcriptional profiles, motif analysis from the JASPAR database and enrichment of motifs in peaks. Motif analysis was performed using Seurat and Signac pipelines to identify transcription factor motifs within the JASPAR database (2022 version) and determine significantly enriched motif sequences within control and *Uty*^{GT} peaks.

Real-time PCR

Heart tissues were homogenized and lysed in QIAzol lysis reagent (Qiagen, cat. no. 79306), and total RNA was isolated using the RNeasy Mini QIAcube kit (Qiagen, cat. no. 74116). Total RNA was extracted from cells using the RNeasy Mini or RNeasy Micro kit (Qiagen, cat. nos. 74104 and 74004, respectively). One microgram of extracted RNA was reverse transcribed using the High-Capacity cDNA RT kit (Thermo Fisher Scientific, cat. no. 4368814). A QuantStudio 6 Flex PCR machine was used to perform qRT–PCR with Power SYBR Green PCR Master Mix (Applied Biosystems, cat. no. 4367659). Primers for gene expression studies are listed in Supplementary Table 3. *36b4* was used as a reference gene for normalization. Gene expression was evaluated with the ΔΔCt method.

Statistics

GraphPad Prism 8.0 was used for the statistical analyses of all experiments. Data are presented as mean ± s.e.m. The Shapiro–Wilk normality test was used to analyze data normality. Statistical tests included unpaired, two-tailed Student's *t* test (with Welch correction when variance was unequal) for normally distributed data and the Mann–Whitney *U* test for nonnormally distributed data. For multiple comparisons, one-way analysis of

variance (ANOVA) with post hoc Tukey's test (normally distributed data) or the Kruskal–Wallis H test with post hoc Dunn's test (nonnormally distributed data) was performed. Data with more than one variable were evaluated using two-way ANOVA with post hoc Tukey's tests. Sequential data were evaluated using two-way repeated-measures ANOVA with post hoc Sidak or Tukey's multiple-comparison tests. P values were considered significantly different at 0.05 (*$P < 0.05$, **$P < 0.01$, ***$P < 0.001$, ****$P < 0.0001$). Statistical tests performed in each figure are summarized in Supplementary Tables 4 and 5.

Reporting summary

Further information on research design is available in the Nature Portfolio Reporting Summary linked to this article.

Extended Data

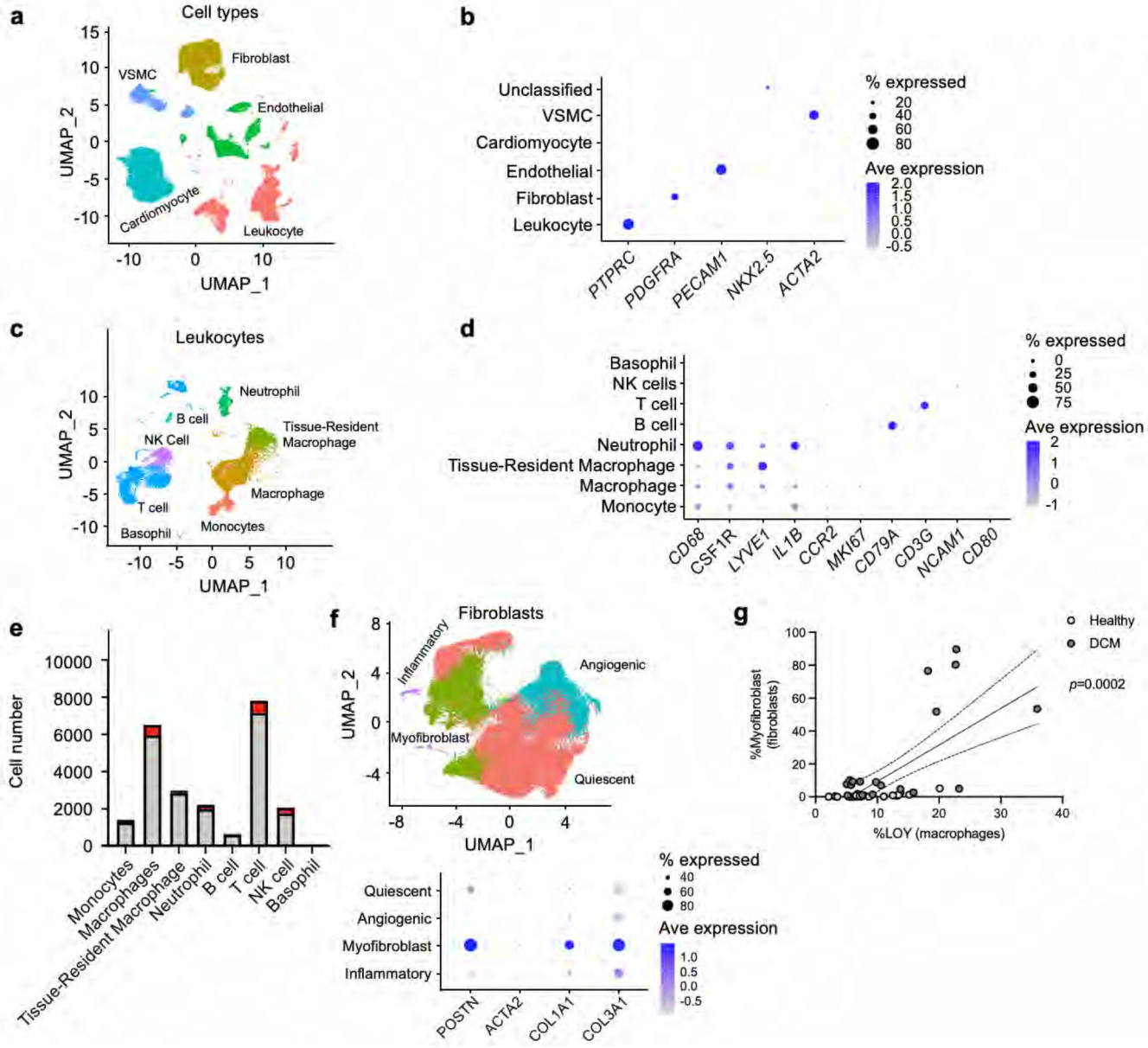

Extended Data Fig. 1 |. Hematopoietic LOY in human dilated cardiomyopathy scRNA-Seq datasets.

a. UMAP dimensionality reduction of annotated cardiac cells from integrated scRNA-Seq datasets (Koenig NCVR 2022, Rao BRC 2021, Chaffin Nature 2022). **b**. Expression of cell type-specific genes used for annotation. **c**. UMAP of annotated cardiac leukocytes. **d**. Expression of cell type-specific genes used for annotation. **e**. Total number of control and LOY leukocytes within each leukocyte subtype (gray = control, red = LOY). **f**. UMAP of annotated cardiac fibroblasts with expression of cell type-specific genes used for myofibroblast annotation. **g**. Linear correlation of myofibroblast percentage within each patient and LOY percentage within each patient, presented by disease.

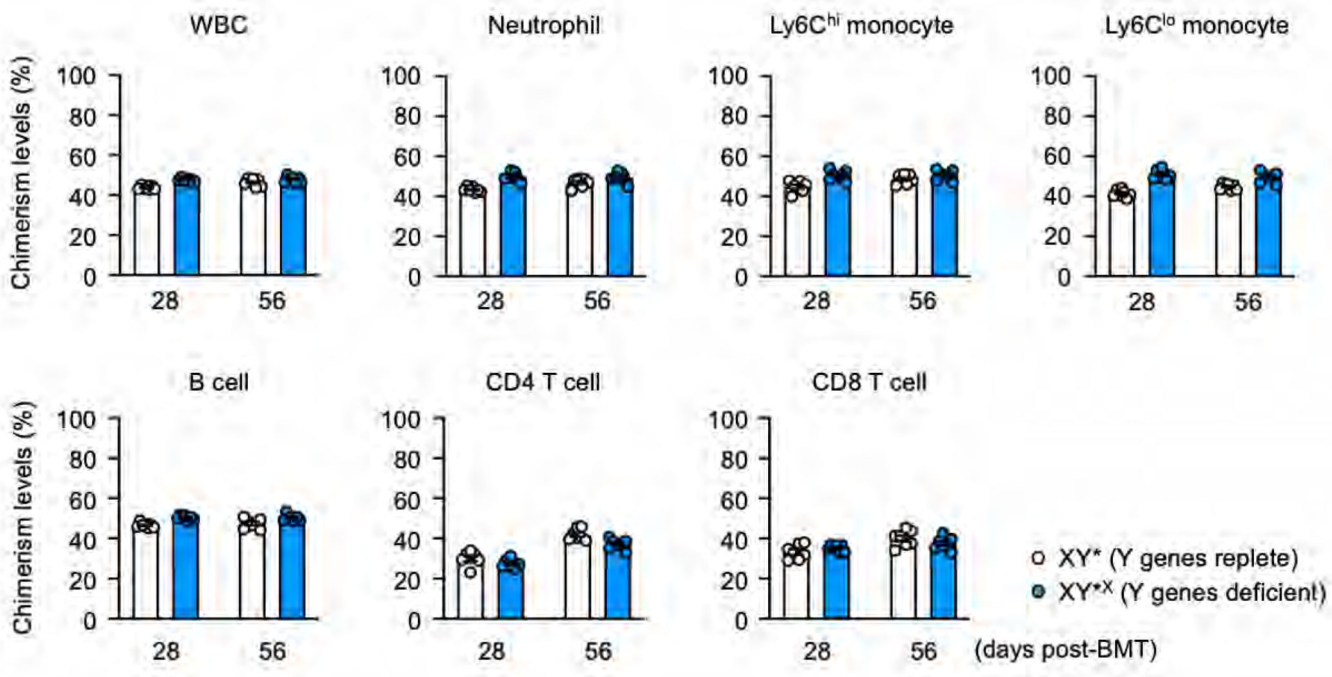

Extended Data Fig. 2 |. Hematopoietic cells with Y chromosome gene deficiency do not display fitness advantage *in vivo*.

Mice underwent partial (50%) bone marrow reconstitution with XY* and XY*^{X} cells following lethal irradiation. After 4 weeks and 8 weeks of recovery, flow cytometric analysis of peripheral blood was performed. (XY* n = 7, XY*^{X} n = 7). Data are presented as mean values +/− SEM. WBC; white blood cells.

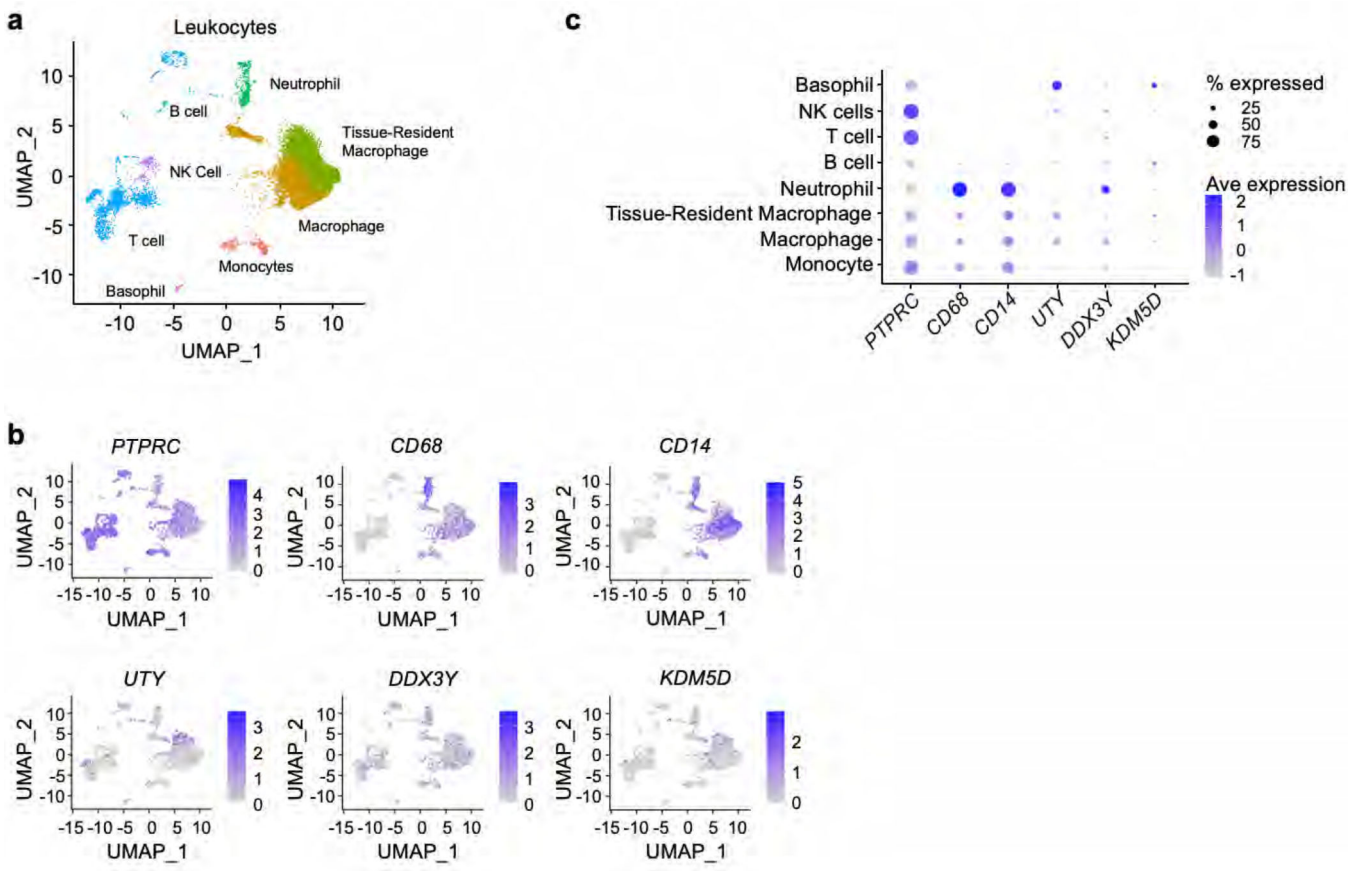

Extended Data Fig. 3 |. Hematopoietic LOY in human healthy cardiac scRNA-Seq datasets.
a. UMAP dimensionality reduction of annotated cardiac cells from integrated scRNA-Seq datasets of healthy male patients. **b-c.** Expression of markers for immune cells (*PTPRC*), monocytes/macrophages (*CD68*, *CD14*), and Y chromosome genes (*UTY*, *DDX3Y*, *KDM5D*), visualized on **(B)** UMAP dimensionality reduction plots, and **(C)** relative expression between cell types.

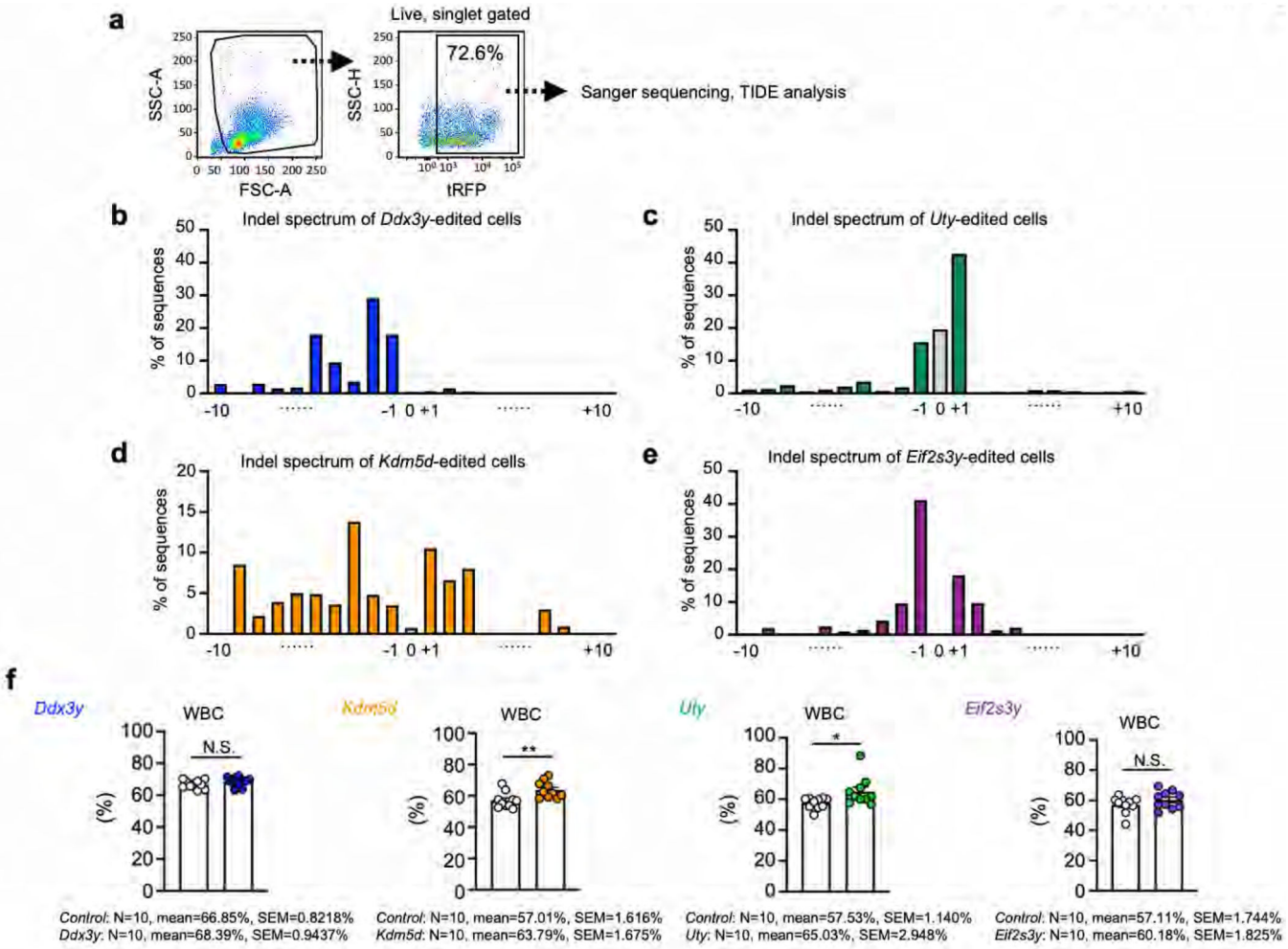

Extended Data Fig. 4 |. CRISPR/Cas9-mediated gene disruption of Y chromosome genes in bone marrow lineage-negative cells.

a. Gating strategy used for the Fluorescence-Activated Cell Sorting (FACS) of peripheral blood cells. Cells transduced with lentivirus transduced cells are designed to express turbo red fluorescent protein (tRFP). **b-e**. The results of Tracking of Indels by Decomposition (TIDE) analysis of sorted cells revealed the presence of multiple insertions and deletions in *Ddx3y* (**b**), *Uty* (**c**), *Kdm5d* (**d**), *Eif2s3y* (**e**) genes. **f**. Percentage of tRFP-positive cells in blood following BMT in the different gene-editing screens (n = 10 for all conditions, statistical analysis by Student's *t* test). Data are presented as mean values +/− SEM.

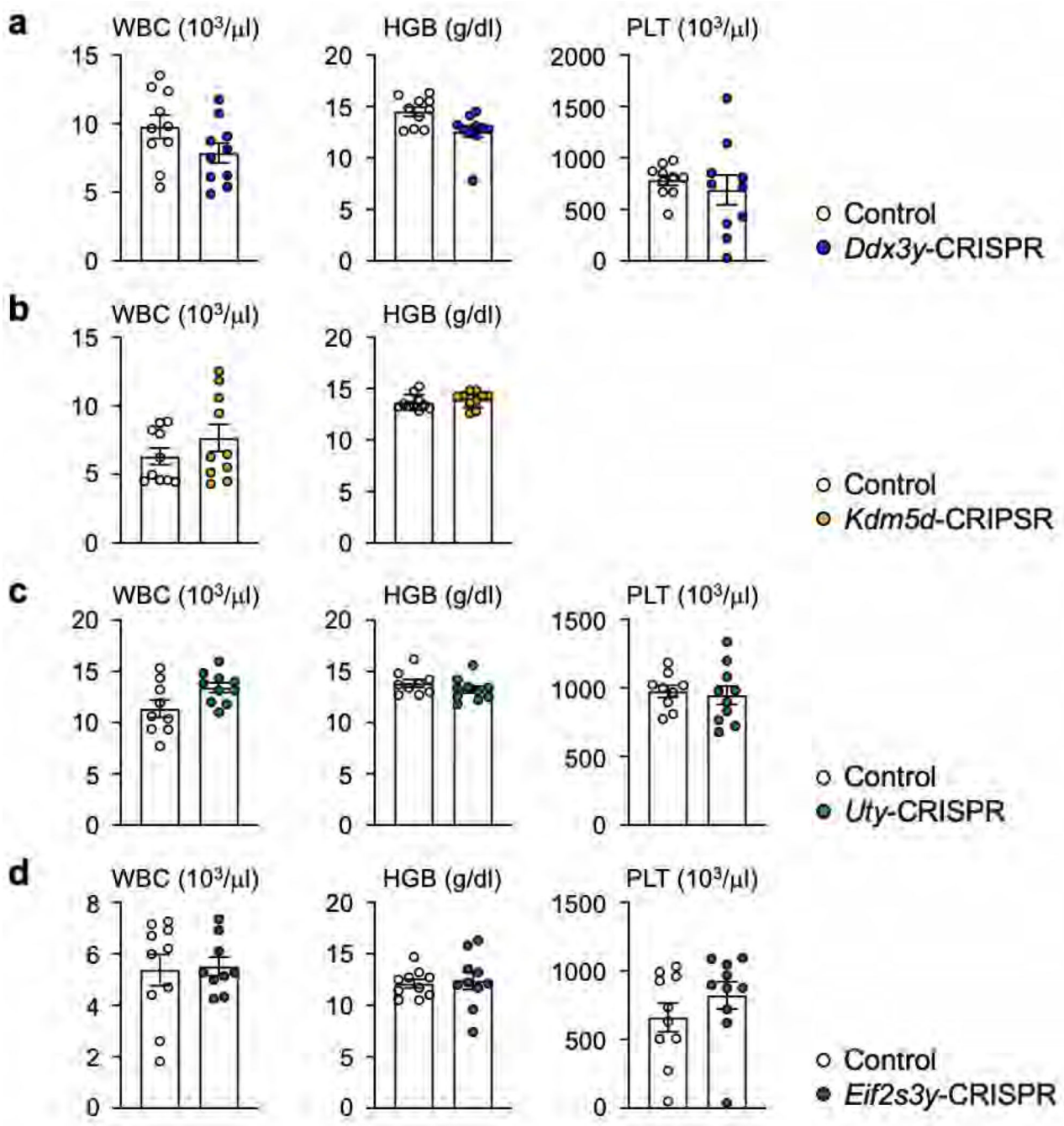

Extended Data Fig. 5 |. Hematopoietic parameters remain unaffected by CRISPR/Cas9-mediated disruption of hematopoietic Y chromosome genes (Ddx3y, Kdm5d, Uty, Eif2s3y).

White blood cell count, hemoglobin concentration, and platelet count were assessed at 4 months (**a**, **b**, **d**) and 1 month (**c**) post-bone marrow transplant (n$=$10 for all conditions). Data are presented as mean values +/− SEM. WBC; white blood cell, HGB; hemoglobin, PLT; platelet.

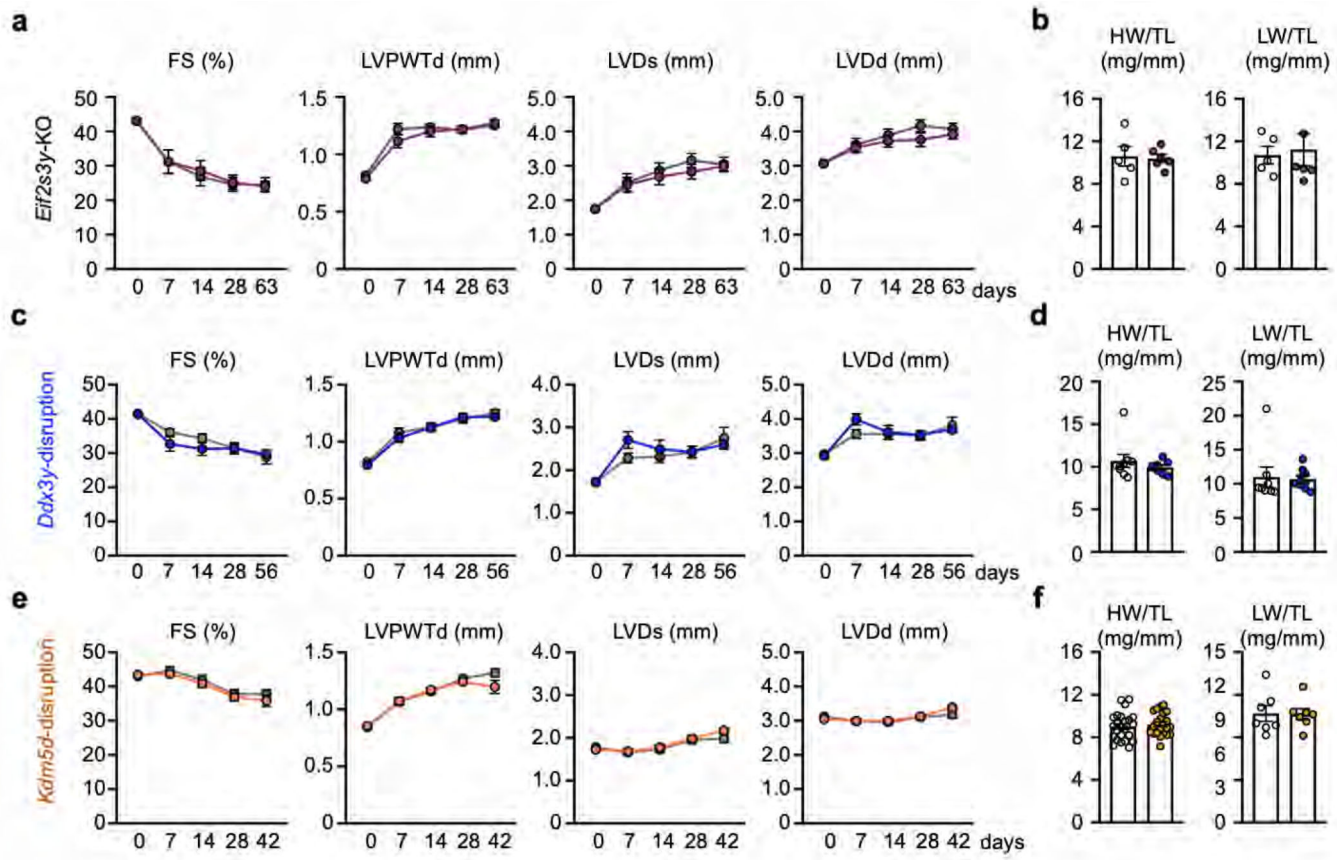

Extended Data Fig. 6 |. CRISPR/Cas9-mediated disruption of hematopoietic *Eif2s3y*, *Ddx3y*, or *Kdm5d* genes do not promote cardiac dysfunction after TAC.

a, c and e. Sequential echocardiographic analysis of KO mice and control mice after TAC at the indicated time points (**a**: control, n = 6; Eif2s3y-KO, n = 6, **c:** control n = 10, Ddx3y-KO n = 8, e: control n = 25, Kdm5d-KO n = 23). **b, d** and **f.** Heart weight (HW) and lung weight (LW) relative to tibia length (TL) at 28 days after TAC procedure (**b-HW/TL**; control, n = 5; Eif2s3y-KO, n = 6, **b-LW/TL**; control, n = 5; Eif2s3y-KO, n = 6, **d-HW/TL**: control n = 9, Ddx3y-KO n = 8, **d-LW/TL**: control n = 8, Ddx3y-KO n = 8, **f-HW/TL**: control n = 24, Kdm5d-KO n = 21, **f-LW/TL**: control n = 7, Kdm5d-KO n = 7). Data are presented as mean values +/− SEM.

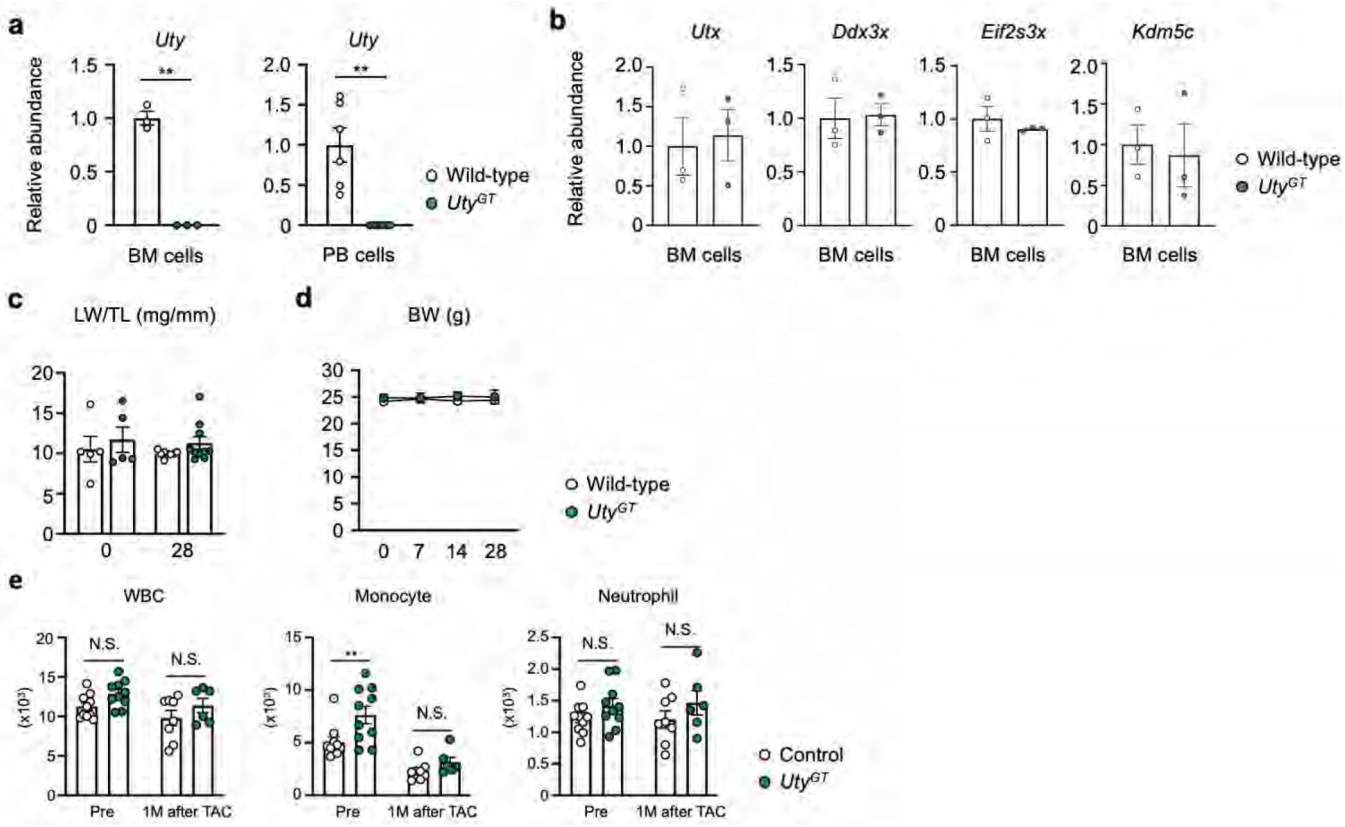

Extended Data Fig. 7 |. *Uty* expression and X chromosome paralogs in hematopoietic cells of *UtyGT* mice.

a. Transcript levels of *Uty* in total bone marrow cells (BM, wild-type n = 3, Uty^{GT} n = 3, Student's *t* test) and whole peripheral blood cells (PB, wild-type n = 5, Uty^{GT} n = 5, Student's *t* test). **b**. Transcript levels of *Utx*, *Ddx3x*, *Eif2s3x*, and *Kdm5c* in BM cells (n = 3 for all conditions). After TAC, lung weight, body weight and blood cell counts in wild-type mice and Uty^{GT} mice were determined. **c**. Lung weight relative to tibial length at 0 and 28 days after TAC procedure. (Day 0: wild-type n = 5, Uty^{GT} n = 5, Day 28: wild-type n = 10, Uty^{GT} n = 10). **d**. Body weight over the time course after TAC (wild-type n = 10, Uty^{GT} n = 10). LW; lung weight, TL: tibial length, BW; body weight. **e**. Flow cytometry was performed at baseline and 1 month post-TAC to determine cell counts in peripheral blood (Pre: Control n = 9, Uty^{GT} n = 9, 1 M after TAC: Control n = 8, Uty^{GT} n = 6, statistical analysis by two-way ANOVA post hoc Tukey). Data are presented as mean values +/− SEM, p-values: N.S.=not significant, *<0.05, **<0.01. BM; bone marrow, PB; peripheral blood; WBC; white blood cells.

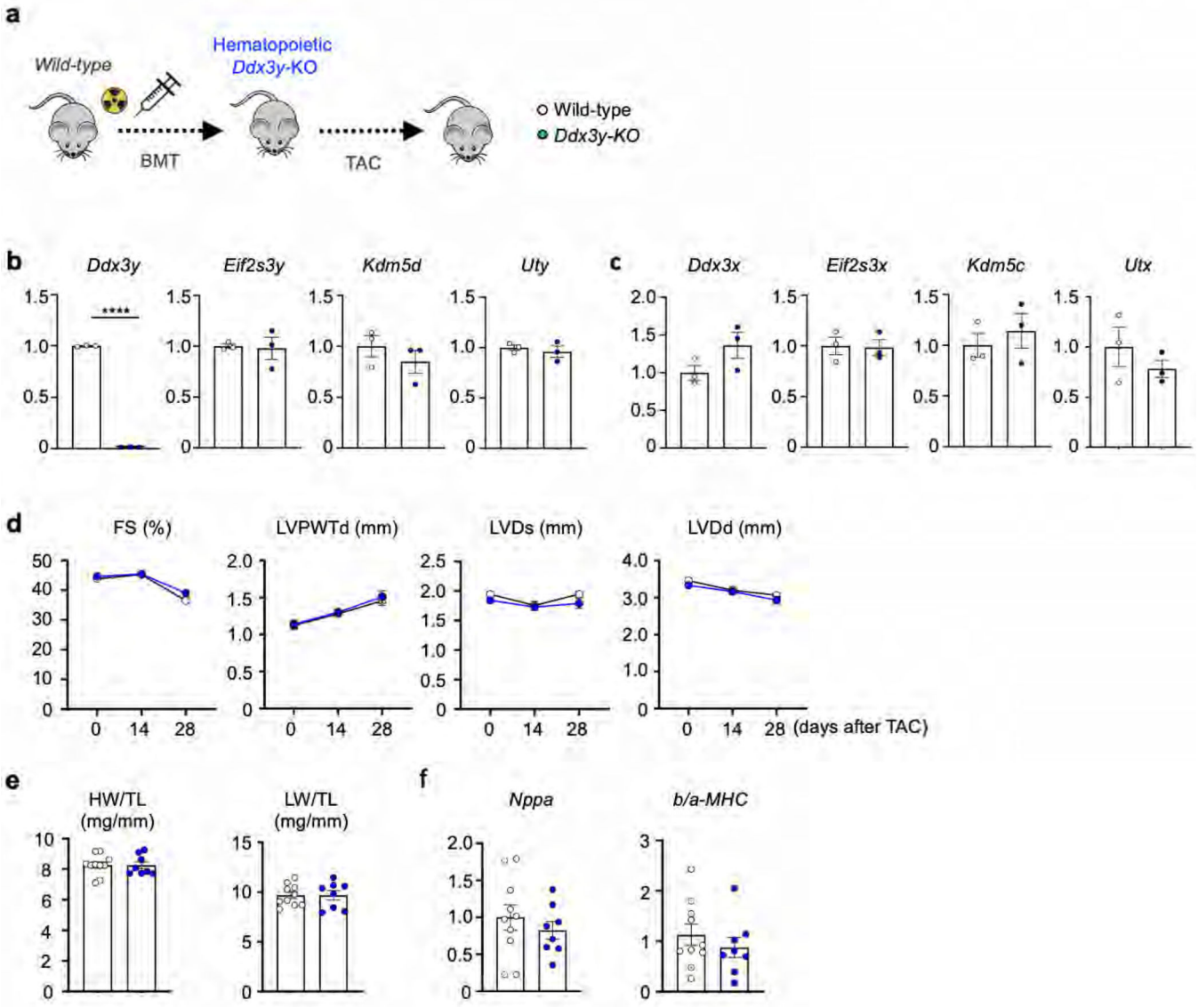

Extended Data Fig. 8 |. Transgenic-mediated Ddx3y-KO of hematopoietic cells does not promote cardiac dysfunction after TAC.

a. Schematic of experimental procedure. **b**. Transcript levels of the Y chromosome genes (*Eif2s3y*, *Ddx3y*, *Kdm5d*, *Uty*) in bone marrow cells (wild-type n = 3, Ddx3y-KO n = 3). **c**. Transcript levels of the X chromosome gene homologues (*Eif2s3x*, *Ddx3x*, *Kdm5c*, *Utx*) in white blood cells isolated from bone marrow from either group of mice (wild-type n = 3, Ddx3y-KO n = 3). **d**. Sequential echocardiographic analysis of mice transplanted with wild-type or Ddx3y-KO cells. Repeated measurement was performed at the indicated time points after TAC operation (wild-type, n = 10; Ddx3y-KO, n = 8). **e**. Heart weight (HW) and lung weight (LW) relative to tibial length (TL) at 4 weeks after TAC procedure (HW/TL; control, n = 10; Ddx3y-KO, n = 8, LW/TL; wild-type, n = 10; Ddx3y-KO, n = 8). **f**. Transcript levels of heart failure markers in heart tissue at four weeks after TAC operation (wild-type, n = 10; Ddx3y-KO, n = 8). Statistical analyses were performed using 2-way ANOVA with Sidak's multiple comparison tests **d**. and two-sided unpaired Student's

t test (**b**, **c**, **e**, **f**). TAC; transverse aortic constriction, FS; fractional shortening, LVPWTd; left ventricular posterior wall thickness at end-diastole, LVDs; left ventricular diameter at end-systole, LVDd; left ventricular diameter at end-diastole. Dots in all panels represent individual samples. Data are shown as mean ± SEM.

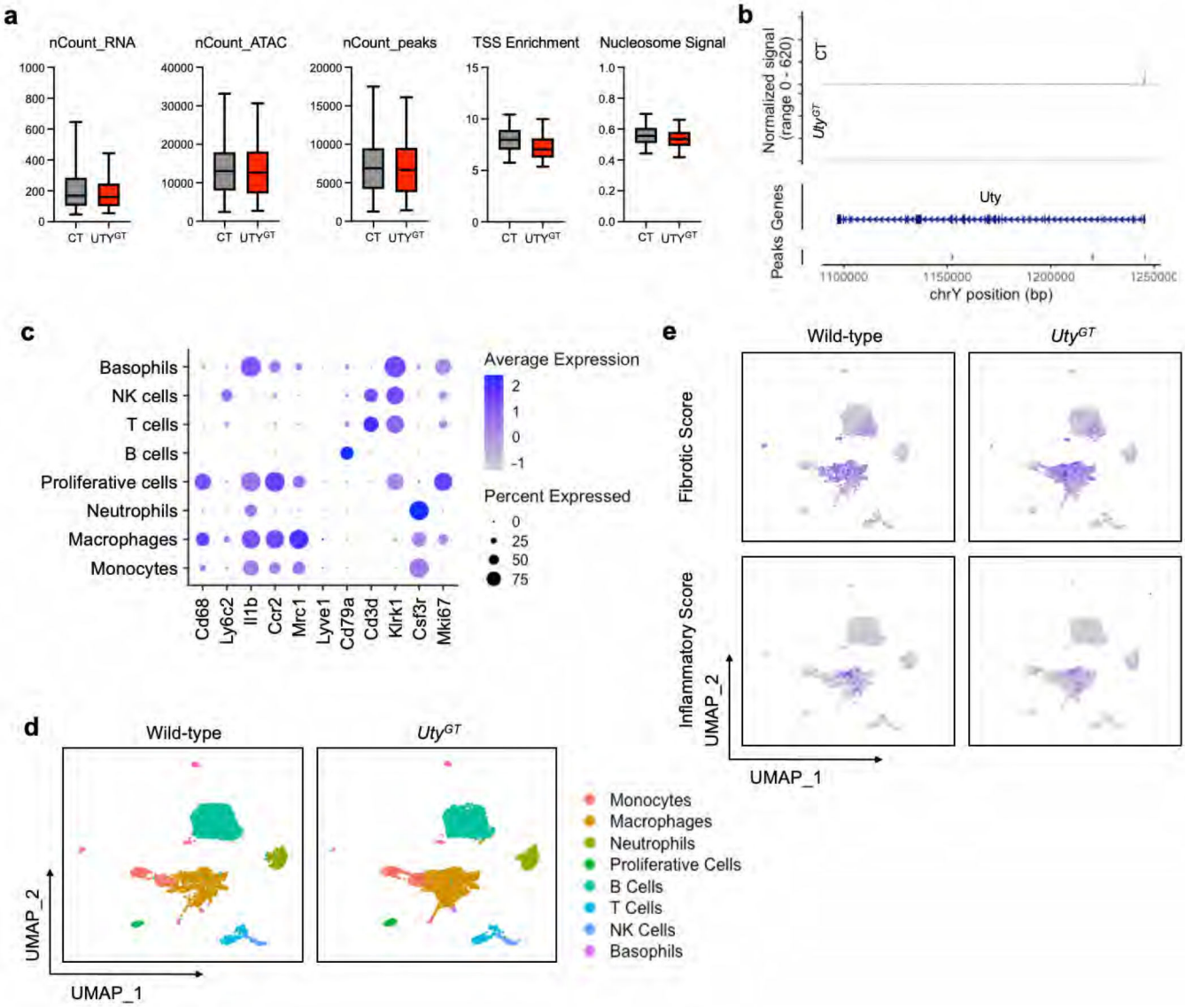

Extended Data Fig. 9 |. Multi-modal single-cell omics of recruited *Uty*^{GT} cardiac leukocytes.
a. Quality control metrics for single cell muiltiomics dataset: RNA reads per cell (nCount_RNA), ATAC reads per cell (nCount_ATAC), quantified peaks per cell (nCount_peaks), enrichment of ATAC reads near transcriptional start sites (TSS Enrichment), nucleosome banding pattern (nucleosome_signal) (box plots: min 25%, max 75%, middle median, whiskers 5%−95%, Control n = 8156, *Uty*^{GT} n = 9169). **b**. DNA accessibility coverage plot for the Uty locus in Control and UTY^{GT} samples showing ATAC reads and calculated peaks. **c**. Expression of known genes that are enriched in specific leukocyte cell types used to annotate clusters of single cells within the single-cell

multiomics dataset. **d**. UMAP dimensionality reduction of wild-type and *Uty*^{GT} cardiac leukocytes based on differential chromatin availability around genes. **e**. Scoring of each cell on increased chromatin availability around genes associated with fibrotic macrophages (Fibrotic Score) or inflammatory macrophages (Inflammatory Score), plotted by UMAP position.

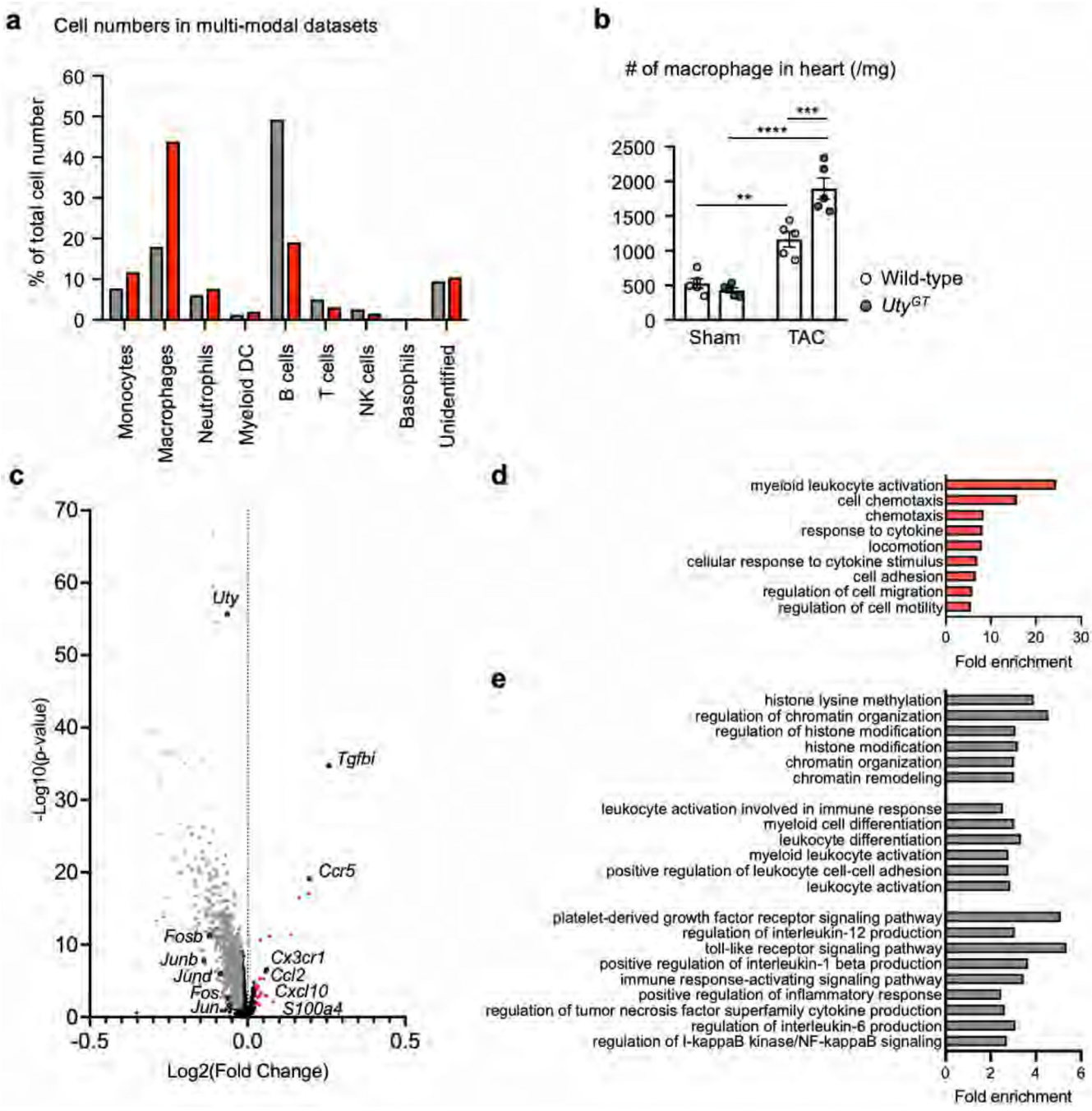

Extended Data Fig. 10 |. Abundance of monocytes and macrophages in the hearts from control and *Uty*^{GT} mice after TAC.

a. Relative abundance of monocytes and macrophages in datasets from control and Uty^{GT} hearts quantified by percentage of total cell number. **b**. Flow cytometric analysis of macrophage counts in heart tissue 28 days after TAC. The absolute numbers of cells were normalized by tissue weight (Sham: wild-type n = 5, Uty^{GT} n = 5; TAC: wild-type n = 5, Uty^{GT} n = 5, data are presented as mean values +/− SEM, two-way ANOVA post hoc Tukey, p-value: **<0.01, ***<0.001, ****<0.0001). **c**. Variation in expression of each gene between Control and Uty^{GT} monocytes and macrophages plotted as -Log10(p-value) versus Log2(Fold Change) (Wilcoxon Rank Sum statistical test). **d, e**. Gene Ontology terms significantly enriched in significant differentially expressed genes monocytes and macrophages (**d:** enriched in Uty^{GT} cells, **e:** enriched in Control cells).

Supplementary Material

Refer to Web version on PubMed Central for supplementary material.

Acknowledgements

This work was supported by National Institutes of Health (NIH) grants AG073249 and HL142650 and National Aeronautics and Space Administration grant 80NSSC21K0549 to K.W.; NIH grant HL152174 to S.S. and K.W.; the University of Virginia Medical Scientist Training Program (T32GM007267) to J.D.C.; American Heart Association grant 23CDA1054358 to N.W.C.; Grant-in-Aid for Research Activity Start-up (21K20879) to S.S.; Grant-in-Aid for Scientific Research (22K08162) to S.S.; Grant for Basic Research of the Japanese Heart Failure Society to S.S.; Grant for Basic Research of the Japanese Circulation Society to S.S.; Research Grant of the Japan Cardiovascular Research Foundation to S.S.; Research Grant of the SENSHIN Medical Research Foundation to S.S.; Research Grant of the MSD Life Science Foundation to S.S.; Novartis research grant to S.S.; Research Grant of the Kondou Kinen Medical Foundation to S.S.; and the Bayer Scholarship for Cardiovascular Research to S.S. We would like to thank X. Chen and H. Hrncir (Department of Integrative Biology and Physiology, University of California, Los Angeles, Los Angeles, CA, USA) for technical assistance. We acknowledge the use of Servier Medical Art, as Fig. 5a was partially generated using Servier Medical Art, provided by Servier, licensed under a Creative Commons Attribution 3.0 unported license. Some illustrations (Fig. 3a and Supplementary Fig. 1) were created with BioRender.com. This research was made possible by the University of Virginia Flow Cytometry Core (RRID: SCR_017829) and Genome Analysis and Technology Core (RRID: SCR_018883).

Data availability

All data supporting the findings in this study are included in the main article and associated files. Single-cell multiomics raw sequencing data and processed data files used to generate and perform analyses of control and Uty^{GT} cardiac leukocytes are available in the NCBI GEO repository under accession no. GSE241486. Additional analyses used datasets available in the NCBI GEO repository under accession nos. GSE183852 and GSE145154 and the Broad Institute Single Cell Portal under accession no. SCP1303. Source data are provided with this paper.

References

1. Thompson DJ et al. Genetic predisposition to mosaic Y chromosome loss in blood. Nature 575, 652–657 (2019). [PubMed: 31748747]
2. Jacobs PA et al. Change of human chromosome count distributions with age: evidence for a sex difference. Nature 197, 1080–1081 (1963). [PubMed: 13964326]
3. Pierre RV & Hoagland HC Age-associated aneuploidy: loss of Y chromosome from human bone marrow cells with aging. Cancer 30, 889–894 (1972). [PubMed: 4116908]
4. Colaco S. & Modi D. Genetics of the human Y chromosome and its association with male infertility. Reprod. Biol. Endocrinol. 16, 14 (2018). [PubMed: 29454353]

5. Forsberg LA et al. Mosaic loss of chromosome Y in peripheral blood is associated with shorter survival and higher risk of cancer. Nat. Genet. 46, 624–628 (2014). [PubMed: 24777449]
6. Haitjema S. et al. Loss of Y chromosome in blood is associated with major cardiovascular events during follow-up in men after carotid endarterectomy. Circ. Cardiovasc. Genet. 10, e001544 (2017).
7. Mas-Peiro S. et al. Mosaic loss of Y chromosome in monocytes is associated with lower survival after transcatheter aortic valve replacement. Eur. Heart J. 44, 1943–1952 (2023). [PubMed: 36932691]
8. Sano S. et al. Hematopoietic loss of Y chromosome leads to cardiac fibrosis and heart failure mortality. Science 377, 292–297 (2022). [PubMed: 35857592]
9. Dumanski JP et al. Immune cells lacking Y chromosome show dysregulation of autosomal gene expression. Cell. Mol. Life Sci. 78, 4019–4033 (2021). [PubMed: 33837451]
10. Chaffin M. et al. Single-nucleus profiling of human dilated and hypertrophic cardiomyopathy. Nature 608, 174–180 (2022). [PubMed: 35732739]
11. Koenig AL et al. Single-cell transcriptomics reveals cell-type-specific diversification in human heart failure. Nat. Cardiovasc. Res. 1, 263–280 (2022). [PubMed: 35959412]
12. Rao M. et al. Resolving the intertwining of inflammation and fibrosis in human heart failure at single-cell level. Basic Res. Cardiol. 116, 55 (2021). [PubMed: 34601654]
13. Daseke MJ 2nd et al. Cardiac fibroblast activation during myocardial infarction wound healing: fibroblast polarization after MI. Matrix Biol. 91–92, 109–116 (2020).
14. Mouton AJ et al. Fibroblast polarization over the myocardial infarction time continuum shifts roles from inflammation to angiogenesis. Basic Res. Cardiol. 114, 6 (2019). [PubMed: 30635789]
15. Burgoyne PS & Arnold AP A primer on the use of mouse models for identifying direct sex chromosome effects that cause sex differences in non-gonadal tissues. Biol. Sex Differ. 7, 68 (2016). [PubMed: 27999654]
16. Chavkin NW et al. The cell surface receptors Ror1/2 control cardiac myofibroblast differentiation. J. Am. Heart Assoc. 10, e019904 (2021).
17. Wang Y. et al. Wnt5a-mediated neutrophil recruitment has an obligatory role in pressure overload-induced cardiac dysfunction. Circulation 140, 487–499 (2019). [PubMed: 31170826]
18. Soh YQS et al. Sequencing the mouse Y chromosome reveals convergent gene acquisition and amplification on both sex chromosomes. Cell 159, 800–813 (2014). [PubMed: 25417157]
19. Skelly DA et al. Single-cell transcriptional profiling reveals cellular diversity and intercommunication in the mouse heart. Cell Rep. 22, 600–610 (2018). [PubMed: 29346760]
20. Sano S. et al. Lentiviral CRISPR/Cas9-mediated genome editing for the study of hematopoietic cells in disease models. J. Vis. Exp. 10.3791/59977 (2019).
21. Chu VT et al. Efficient CRISPR-mediated mutagenesis in primary immune cells using CrispRGold and a C57BL/6 Cas9 transgenic mouse line. Proc. Natl Acad. Sci. USA 113, 12514–12519 (2016). [PubMed: 27729526]
22. Shpargel KB, Sengoku T, Yokoyama S. & Magnuson T. UTX and UTY demonstrate histone demethylase-independent function in mouse embryonic development. PLoS Genet. 8, e1002964 (2012).
23. Park E. et al. Bone marrow transplantation procedures in mice to study clonal hematopoiesis. J. Vis. Exp. 10.3791/61875 (2021).
24. Wang Y. et al. Tet2-mediated clonal hematopoiesis in nonconditioned mice accelerates age-associated cardiac dysfunction. JCI Insight 5, e135204 (2020).
25. Matsumura T. et al. An azoospermic factor gene, Ddx3y and its paralog, Ddx3x are dispensable in germ cells for male fertility. J. Reprod. Dev. 65, 121–128 (2019). [PubMed: 30613052]
26. Shi B. et al. UTX condensation underlies its tumour-suppressive activity. Nature 597, 726–731 (2021). [PubMed: 34526716]
27. Walport LJ et al. Human UTY(KDM6C) is a male-specific Nϵ-methyl lysyl demethylase. J. Biol. Chem. 289, 18302–18313 (2014). [PubMed: 24798337]
28. Conlon FL & Arnold AP Sex chromosome mechanisms in cardiac development and disease. Nat. Cardiovasc. Res. 2, 340–350 (2023). [PubMed: 37808586]

29. Sano S, Thel MC & Walsh K. Mosaic loss of Y chromosome in white blood cells: its impact on men's health. Physiology (Bethesda) 38, 0 (2023).
30. Li R. & Zhu J. Effects of aneuploidy on cell behaviour and function. Nat. Rev. Mol. Cell Biol. 23, 250–265 (2022). [PubMed: 34987171]
31. Zhang Q. et al. Mosaic loss of chromosome Y promotes leukemogenesis and clonal hematopoiesis. JCI Insight 7, e153768 (2022).
32. Abdel-Hafiz HA et al. Y chromosome loss in cancer drives growth by evasion of adaptive immunity. Nature 619, 624–631 (2023). [PubMed: 37344596]
33. Hao Y. et al. Integrated analysis of multimodal single-cell data. Cell 184, 3573–3587 (2021). [PubMed: 34062119]
34. Sano S. & Walsh K. Development of a mouse model of hematopoietic loss of Y chromosome. Bio-protocol 13, e4729 (2023). [PubMed: 37575386]
35. Wang Y. et al. Murine models of clonal haematopoiesis to assess mechanisms of cardiovascular disease. Cardiovasc. Res. 118, 1413–1432 (2022). [PubMed: 34164655]
36. Stuart T. et al. Single-cell chromatin state analysis with Signac. Nat. Methods 18, 1333–1341 (2021). [PubMed: 34725479]
37. Feng J. et al. Identifying ChIP–seq enrichment using MACS. Nat. Protoc. 7, 1728–1740 (2012). [PubMed: 22936215]
38. van Dijk D. et al. Recovering gene interactions from single-cell data using data diffusion. Cell 174, 716–729 (2018). [PubMed: 29961576]

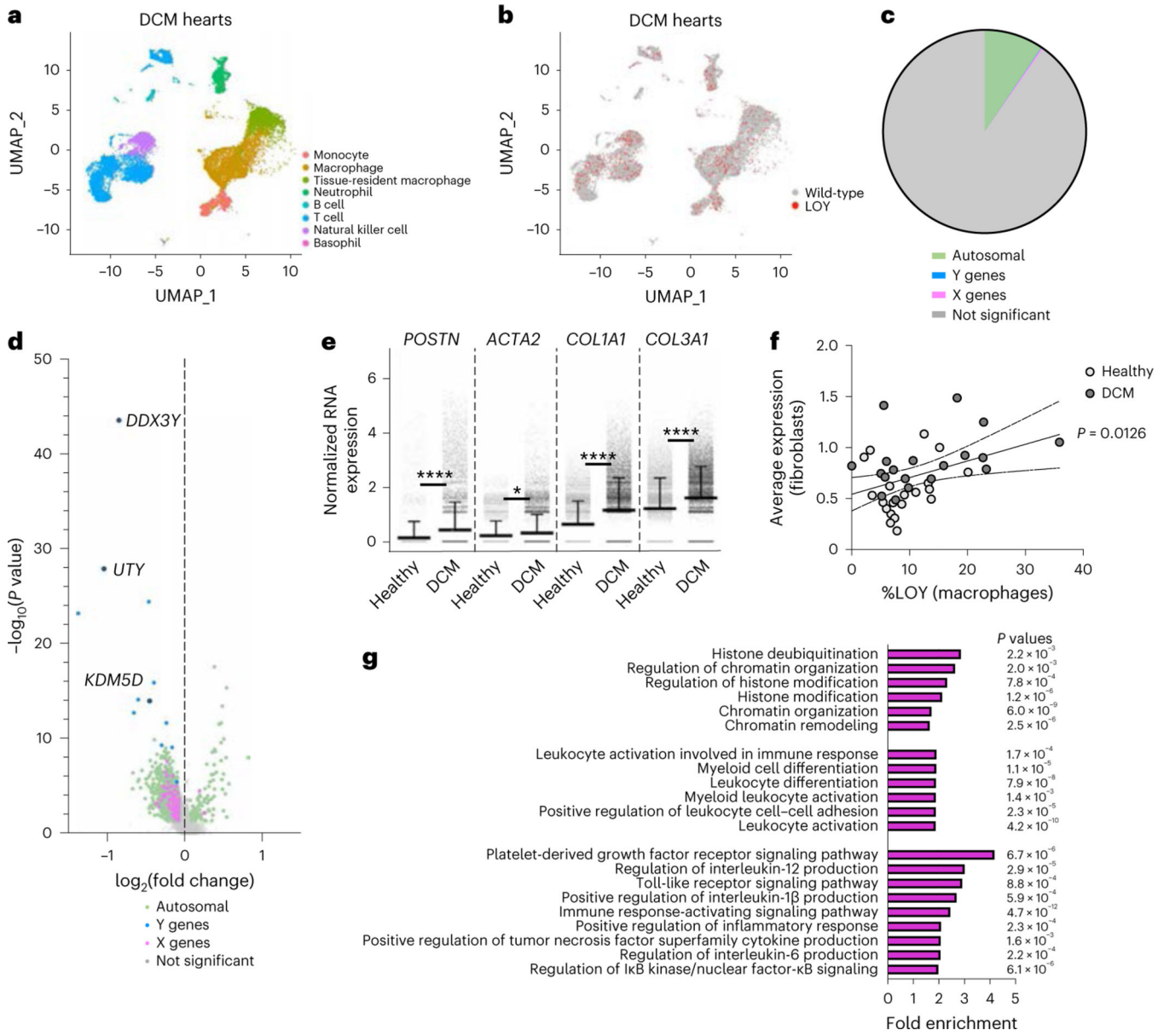

Fig. 1 |. Hematopoietic LOY in human DCM scRNA-Seq datasets.

a, UMAP dimensionality reduction of annotated cardiac leukocytes from integrated scRNA-Seq datasets from male patients with DCM. **b**, Distribution of LOY cells within cardiac leukocyte cell types. **c**, Percentages of significant autosomal genes (9.45%, green), significant Y genes (0.05%, blue), significant X genes (0.28%, pink) and nonsignificant genes (90.22%, gray) over the total expressed genes. **d**, Variation in the expression of each gene between control and LOY cardiac macrophages plotted as $-\log_{10}(P\text{value})$ versus $\log_2$(fold change) (Wilcoxon rank-sum statistical test). **e**, Comparison of the fibroblast activation genes *POSTN*, *ACTA2*, *COL1A1* and *COL3A1* in fibroblasts between healthy patients and patients with DCM (data show the mean normalized RNA expression, with error bars representing the s.d.; two-way ANOVA post hoc Sidak: $*P < 0.05$, $****P < 0.0001$). **f**, Linear correlation of the average expression of fibroblast activation genes and

the LOY percentage within each patient (simple linear regression statistical test). **g**, Gene Ontology terms significantly enriched in significant differentially expressed genes in control versus LOY macrophages of patients with DCM (Fisher's exact statistical test).

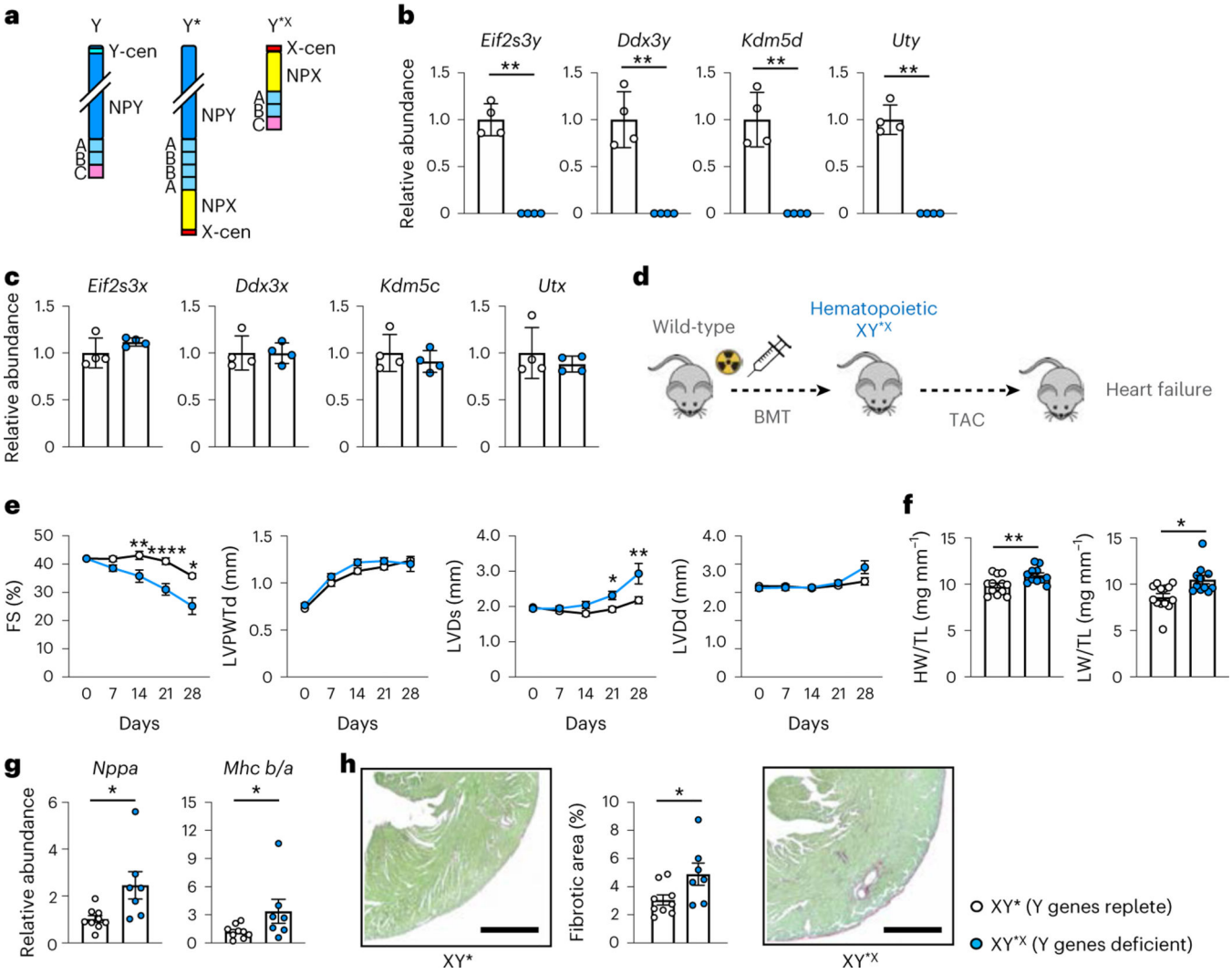

Fig. 2 |. Deficiency of Y chromosome genes in hematopoietic cells exacerbates cardiac dysfunction in response to pressure overload.

a, Illustration of structural differences in the Y chromosome among normal male Y mice, XY* mice and XY*^{X} mice. The ABC portions of the chromosomes are in the PAR. **b**, Transcript levels of the Y chromosome genes *Eif2s3y*, *Ddx3y*, *Kdm5d* and *Uty* in white blood cells isolated from the bone marrow of either group of mice (XY* $n = 4$, XY*^{X} $n = 4$; Student's t test). **c**, Transcript levels of the X chromosome gene homologs (*Eif2s3x*, *Ddx3x*, *Kdm5c*, *Utx*) in white blood cells isolated from the bone marrow of either group of mice (XY* $n = 4$, XY*^{X} $n = 4$). **d**, Schematic illustration of the phenotypic study of Y*^{X} mice in a pressure overload model: lethally irradiated wild-type mice were transplanted with bone marrow cells from either Y* or Y*^{X} mice and subjected to TAC surgery at 6 weeks after BMT. **e**, Sequential echocardiographic analysis of Y* and Y*^{X} mice before and after TAC surgery at the indicated time points (XY* $n = 14$, XY*^{X} $n = 11$; two-way ANOVA post hoc Tukey). **f**, Heart weight and lung weight relative to tibia length at 4 weeks after the TAC procedure (XY* $n = 13$, XY*^{X} $n = 11$; statistical tests: Student's t test (heart weight/tibia length), Mann–Whitney U test (lung weight/tibia length)). **g**, Transcript levels

of heart failure markers (*Nppa* and *Mhc b/a*) in heart tissues at 28 days after TAC surgery (XY* $n = 9$, XY*^{X} $n = 7$; Mann–Whitney U statistical test). **h**, Quantitative analysis of the fibrotic area in heart sections at 4 weeks after TAC surgery (scale bars, 500 μm; XY* $n = 9$, XY*^{X} $n = 7$; Student's t test). Data are presented as mean values ± s.e.m. *$P < 0.05$, **$P < 0.01$, ****$P < 0.0001$. FS, fractional shortening; LVPWTd, left ventricular posterior wall thickness at end-diastole; LVDs, left ventricular diameter at end-systole; LVDd, left ventricular diameter at end-diastole; HW, heart weight; LW, lung weight; TL, tibia length; X-cen, X centromere; Y-cen, Y centromere; NPY, non-PAR of the Y chromosome.

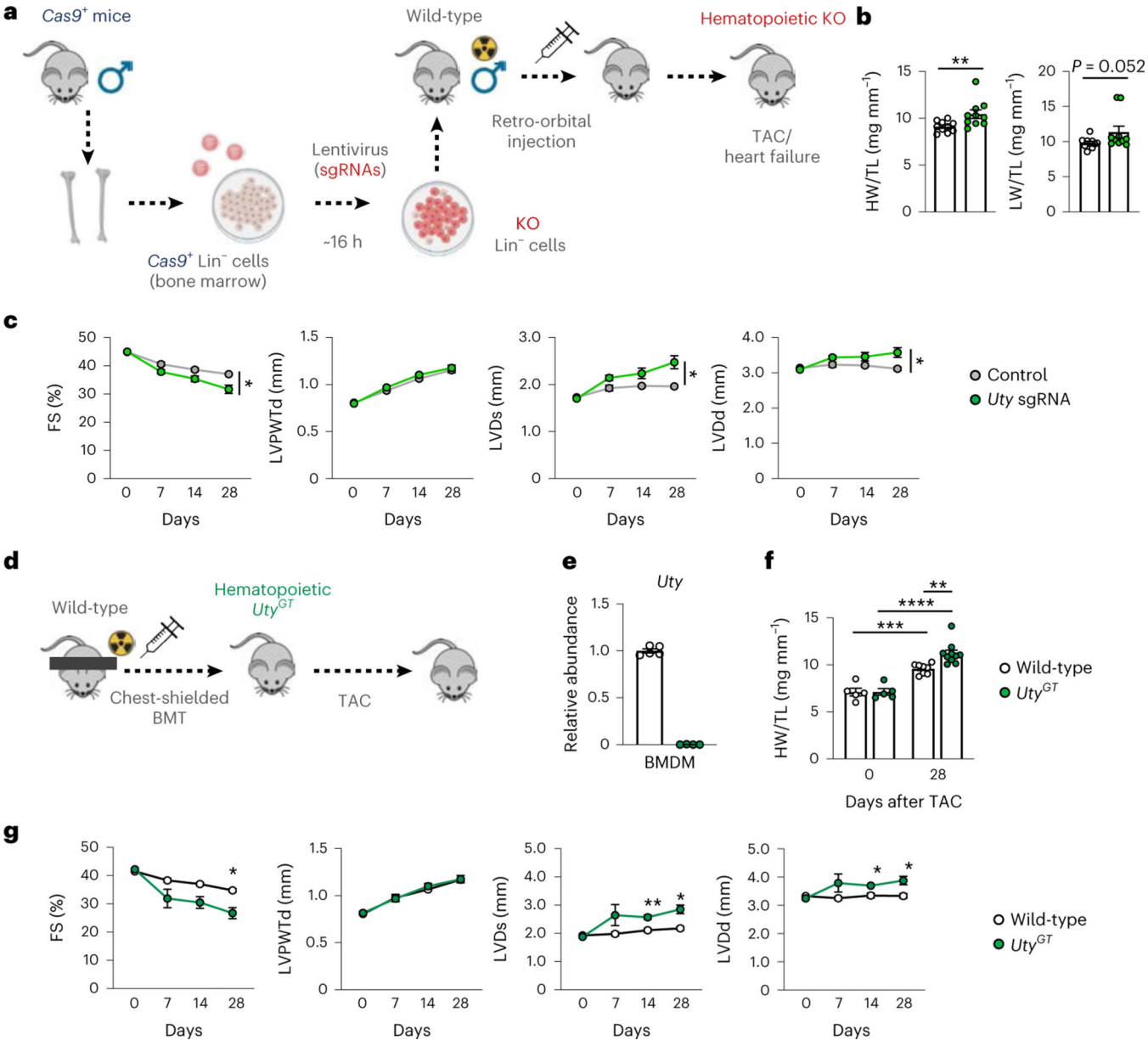

Fig. 3 |. Hematopoietic *Uty* is a potential gene candidate that contributes to LOY-mediated deterioration of cardiac function.

a, Study schematic: lethally irradiated male C57BL/6J mice were reconstituted with hematopoietic lineage-negative cells transduced with a lentivirus encoding the Y chromosome gene-targeting *Uty* gRNA or control gRNA, with analysis of cardiac phenotypes between knockout mice and control mice after TAC surgery. **b**, Heart weight and lung weight relative to tibia length at 28 days after the TAC procedure (heart weight/tibia length and lung weight/tibia length: control $n = 10$, Uty^{GT} $n = 10$; Student's t test). **c**, Sequential echocardiographic analysis of knockout mice and control mice after TAC at the indicated time points (control $n = 10$, Uty^{GT} $n = 10$; two-way repeated-measures ANOVA post hoc Sidak). **d**, Generation of CRISPR/Cas9-free hematopoietic *Uty*-disrupted mice with preserved cardiac microenvironment: male C57BL/6 CD45.1 (Pepboy) mice were lethally

irradiated (with chest shielding) and reconstituted with bone marrow cells collected from Uty^{GT} transgenic (CD45.2) or wild-type (CD45.2) mice. **e**, Transcript levels of *Uty* in bone marrow-derived macrophages (wild-type $n = 5$, Uty^{GT} $n = 4$). **f**, Heart weight relative to tibia length at 0 and 28 days after the TAC procedure (day 0: wild-type $n = 5$, Uty^{GT} $n = 5$, day 28: wild-type $n = 8$, Uty^{GT} $n = 9$; two-way ANOVA post hoc Tukey). **g**, Sequential echocardiographic analysis of mice transplanted with wild-type or Uty^{GT} cells. Repeated measurement was performed at the indicated time points after TAC (wild-type $n = 9$, Uty^{GT} $n = 7$; two-way repeated-measures ANOVA post hoc Sidak). Data are presented as mean values ± s.e.m. $*P < 0.05$, $**P < 0.01$, $***P < 0.001$, $****P < 0.0001$. Lin, lineage; KO, knockout; BMDM, bone marrow-derived macrophage.

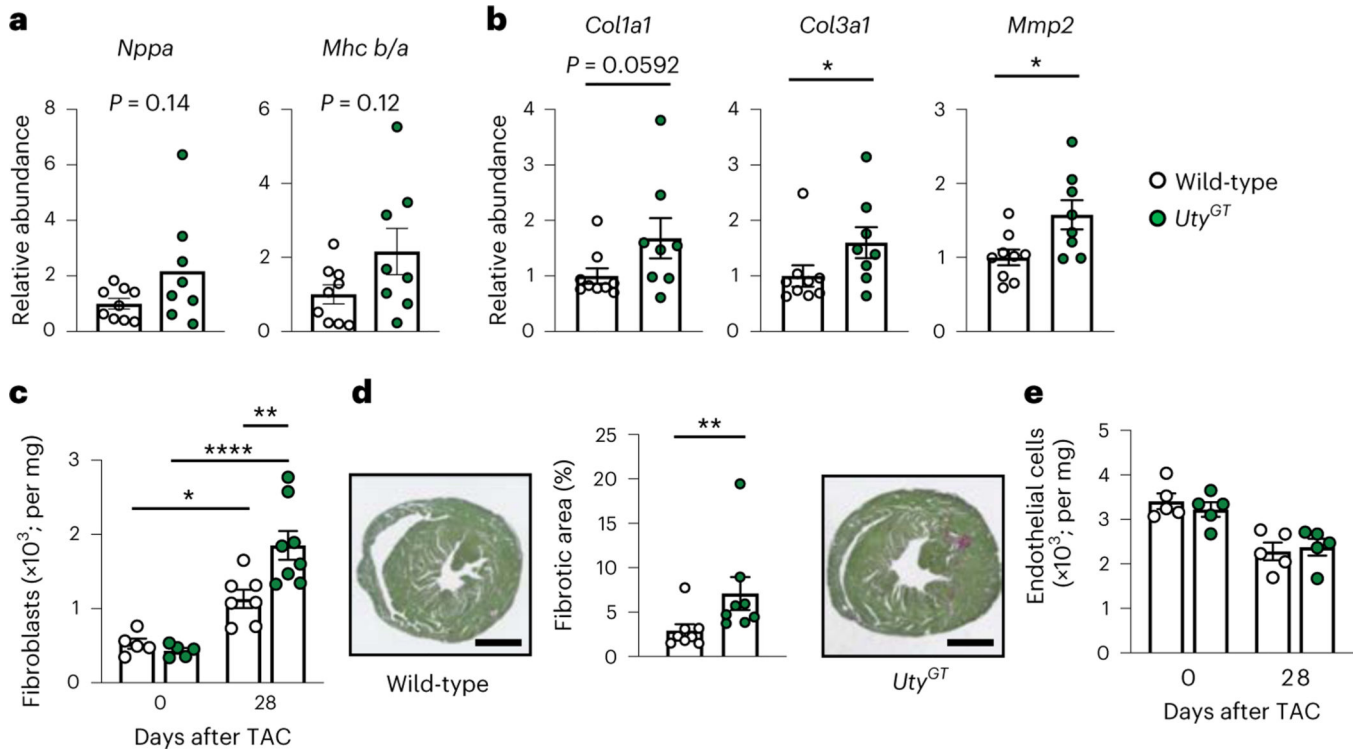

Fig. 4 |. *Uty* disruption in hematopoietic cells accelerates cardiac dysfunction in response to pressure overload.

a, Transcript levels of heart failure markers in heart tissue at 28 days after TAC surgery (wild-type $n = 9$, Uty^{GT} $n = 8$; Student's t test). **b**, Transcript levels of fibrosis markers in heart tissue at 28 days after TAC surgery (wild-type $n = 9$, Uty^{GT} $n = 8$; Student's t test). **c**, Flow cytometric analysis of fibroblast counts in heart tissue at 0 and 28 days after TAC. The absolute numbers of cells were normalized by tissue weight (day 0: wild-type $n = 5$, Uty^{GT} $n = 5$, day 28: wild-type $n = 7$, Uty^{GT} $n = 8$; two-way ANOVA post hoc Tukey). **d**, Quantitative analysis of the fibrotic area in heart sections at 28 days after the TAC operation (scale bars, 1,000 μm; wild-type $n = 6$, Uty^{GT} $n = 8$; Mann–Whitney U test). **e**, Flow cytometric analysis of endothelial cell counts in heart tissue at 0 and 28 days after the TAC operation. The absolute numbers of cells were normalized by tissue weight (day 0: wild-type $n = 5$, Uty^{GT} $n = 5$, day 28: wild-type $n = 5$, Uty^{GT} $n = 5$; two-way ANOVA post hoc Tukey). Data are presented as mean values ± s.e.m. $*P < 0.05$, $**P < 0.01$, $****P < 0.0001$.

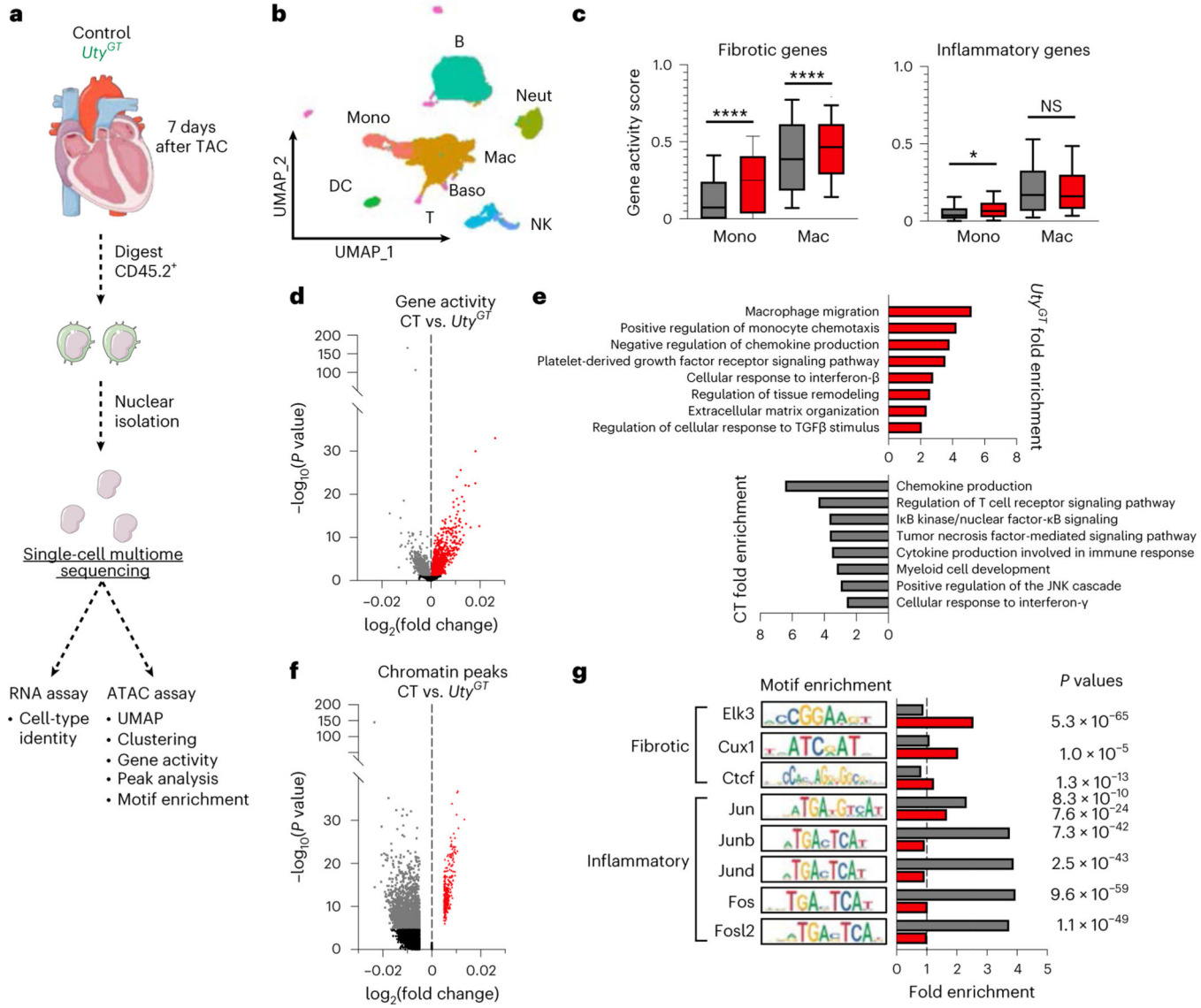

Fig. 5 |. Multimodal single-cell analysis reveals the profibrotic chromatin accessibility signatures of recruited *Uty*^{GT} cardiac monocytes and macrophages.

a, Schematic of the experimental procedure. **b**, UMAP dimensionality reduction based on differential chromatin availability around genes, with all analyzed single cells grouped by annotated cell type. **c**, Chromatin availability around genes associated with fibrotic and inflammatory macrophage transcriptional signatures during myocardial remodeling, quantified in monocytes and macrophages and compared between control (gray) and *Uty*^{GT} (red) hearts (center line, median; box limits, first and third quartiles; whiskers, 10–90% of data; $n = 580$ control monocytes versus 865 *Uty*^{GT} monocytes and 1,404 control macrophages versus 4,716 *Uty*^{GT} macrophages; one-way ANOVA post hoc Tukey: NS, not significant, $*P < 0.05$, $****P < 0.0001$). **d**, Analysis of differential gene availability by chromatin accessibility near genes in monocytes and macrophages, with significantly enriched genes in control (gray) and *Uty*^{GT} (red) cardiac monocytes and macrophages presented as a volcano plot. **e**, Fold enrichment of Gene Ontology terms within gene

sets enriched in Uty^{GT} (red) and control (gray) cardiac monocytes and macrophages. **f**, Analysis of the differential localization of chromatin peaks in monocytes and macrophages enriched in control (gray) and Uty^{GT} (red) hearts, presented as a volcano plot (Wilcoxon rank-sum statistical test). **g**, Motif analysis of the transcription factor-binding sequences of significantly enriched peaks in control (gray) or Uty^{GT} (red) hearts, with the transcription factors associated with fibrotic and inflammatory macrophages presented with the DNA-binding motif and as the fold enrichment of the DNA-binding motifs, with the P values listed (Fisher's exact statistical test). Mono, monocyte; DC, dendritic cell; B, B cell; Neut, neutrophil; Mac, macrophage; Baso, basophil; T, T cell; NK, natural killer cell; CT, control.

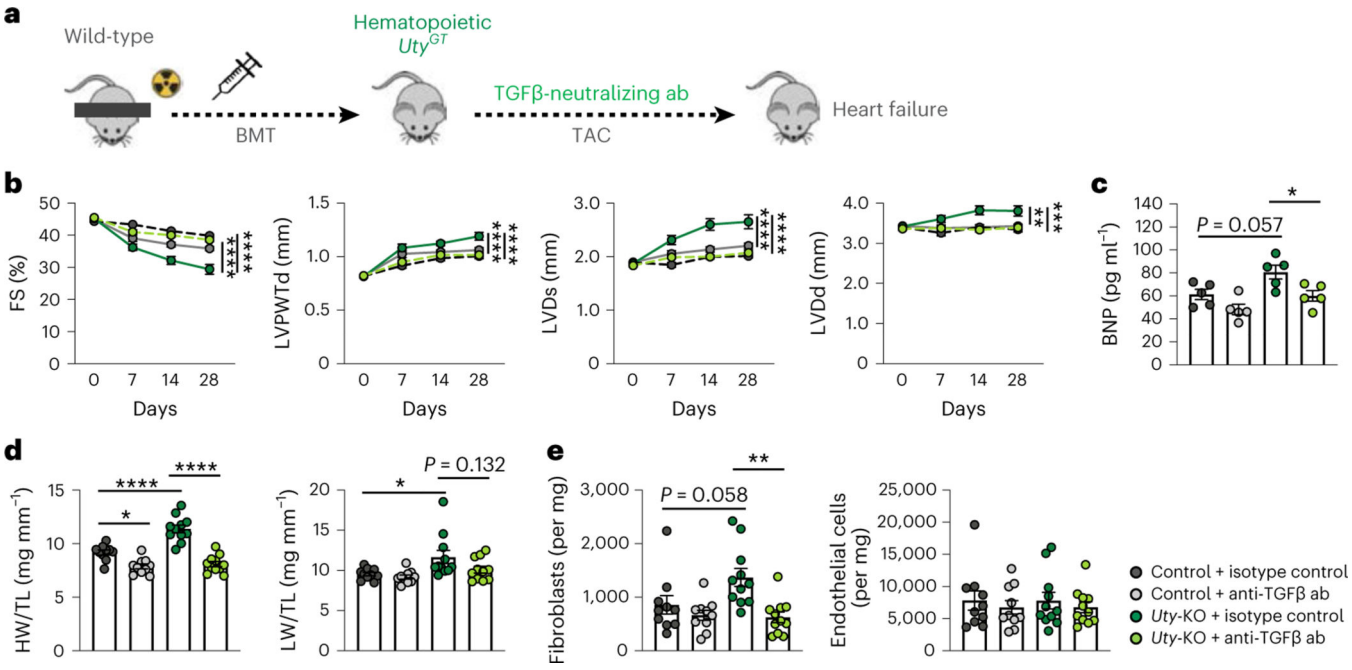

Fig. 6 |. Inhibition of TGFβ reverses cardiac dysfunction after TAC in mice with hematopoietic *Uty* deficiency.

a, Schematic of the experimental procedure. **b**, Sequential echocardiographic analysis of Uty^{GT} and control mice after TAC at the indicated time points. At 8 weeks after BMT, mice were subjected to TAC. An anti-TGFβ antibody or isotype control was intraperitoneally injected every 3 days over the experimental time of 28 days after TAC ($n = 10$ per experimental group). **c**, Serum BNP levels at 28 days after TAC ($n = 5$ per experimental group). **d**, Heart weight and lung weight relative to tibia length at 28 days after TAC ($n = 10$ per experimental group). **e**, Quantitative analysis of flow cytometric data of fibroblast (left) and endothelial cell (right) counts in heart tissue at 28 days after TAC. The absolute numbers of cells were normalized by tissue weight ($n = 10$ per experimental group). Data are presented as mean values ± s.e.m. Statistical analysis was performed by two-way ANOVA with post hoc Tukey's test. *$P < 0.05$, **$P < 0.01$, ***$P < 0.001$, ****$P < 0.0001$. ab, antibody.